JGR Oceans

RESEARCH ARTICLE
10.1029/2024JC021919

Estuarine Exchange Flow in the Albemarle-Pamlico Estuarine System

Dongxiao Yin[1,2], Courtney K. Harris[1], and John C. Warner[3]

[1]Virginia Institute of Marine Science, Gloucester Point, VA, USA, [2]Now at Applied Ocean Physics and Engineering Department, Woods Hole Oceanographic Institution, Woods Hole, MA, USA, [3]U.S. Geological Survey, Woods Hole, MA, USA

Key Points:

- The study of the Albemarle-Pamlico estuarine system (APES) reveals exchange flow dynamics representative of complex coastal lagoons of weak tides
- Exchange flow mechanisms in APES vary by timescale: wind drives short-term, gravitational circulation dominates long-term in tributaries
- Exchange flow may play a key role in controlling the flushing time of the APES, a role that has been previously overlooked

Supporting Information:

Supporting Information may be found in the online version of this article.

Correspondence to:

D. Yin,
dyin@vims.edu;
dongxiao.yin@whoi.edu

Citation:

Yin, D., Harris, C. K., & Warner, J. C. (2025). Estuarine exchange flow in the Albemarle-Pamlico estuarine system. *Journal of Geophysical Research: Oceans*, *130*, e2024JC021919. https://doi.org/10.1029/2024JC021919

Received 29 SEP 2024
Accepted 17 JUL 2025

Author Contributions:

Conceptualization: Dongxiao Yin
Data curation: Dongxiao Yin
Formal analysis: Dongxiao Yin
Funding acquisition: Courtney K. Harris
Investigation: Dongxiao Yin
Methodology: Dongxiao Yin, John C. Warner
Project administration: Courtney K. Harris
Resources: Courtney K. Harris
Software: Dongxiao Yin, John C. Warner
Supervision: Courtney K. Harris
Validation: Dongxiao Yin
Visualization: Dongxiao Yin

Abstract Estuarine exchange flow controls the salt balance and regulates biogeochemistry in an estuary. The Albemarle-Pamlico estuarine system (APES) is the largest coastal lagoon in the U.S. and historically susceptible to a series of environmental issues including salt water intrusion and eutrophication, yet its estuarine exchange flow is poorly understood. Here, we investigate the estuarine exchange flow in the APES, its tributary estuaries (Pamlico and Neuse), and sub-basin Albemarle Sound using the total exchange flow analysis framework based on results from a deterministic numerical model. We find the following: (a) Dynamics controlling estuarine exchange flow in the APES vary spatially and depend on timescales considered. At inlets, estuarine exchange flows respond to both tidal prism and residual water levels at weather-to-spring/neap timescales. At a long quasi-steady timescale represented as annual means, estuarine exchange flow is dominated by barotropic flow. Within the tributary estuaries, estuarine exchange flows at timescales of wind periods are controlled by wind-induced straining, whereas the quasi-steady state condition is dominated by gravitational circulation. At Albemarle Sound, exchange flow is dominated by the residual water levels at weather-to-spring/neap timescales, while at quasi-steady state it is controlled by barotropic flow. (b) At the quasi-steady annual timescale, the salt content decreases with river discharge. At the weather-to-spring/neap timescales, salt content is insensitive to variations in estuarine exchange flow, except for within Albemarle Sound. (c) Estuarine exchange flow likely influences the biogeochemistry of the APES by playing a key role in regulating the flushing efficiency and material exchange, a role that has been previously overlooked.

Plain Language Summary The Albemarle-Pamlico estuarine system (APES) is the largest coastal lagoonal estuary in the U.S. It has faced several environmental problems over the years, like salt water mixing into freshwater areas and excessive nutrients buildup that harm water quality. Understanding water movement in and out of the estuary, that is, "exchange flow", is crucial for addressing these issues. However, this process has not been thoroughly studied, which is why this research is important. For the first time, we used a computer model to systematically analyze how water moves in and out of the APES and its different areas. We found that the factors affecting this movement vary spatially and change depending on the timeframe considered. Over short periods, like less than 2 weeks, tides and weather-induced change in water level are important at the inlets where the APES meets the ocean. Inside the APES, tides are less significant, and winds play a bigger role in moving water around. On a yearly basis, river flow becomes more influential. When river discharge increases, it tends to wash more salt out of the estuary. This water exchange is likely crucial for the biological activities and environmental health of the APES, indicating the need for further study.

1. Introduction

1.1. Estuarine Exchange Flow as an Important Driver of Estuary Salinity and Biogeochemistry

Estuarine exchange flow is the subtidal along-channel volume transport between the estuary and the coastal ocean (MacCready & Geyer, 2014). It accounts for both the landward inflow component and the oceanward outflow component. The landward component brings salty ocean water into the estuary, where it mixes with the freshwater from the river before being carried out of the estuary with intermediate salinity by the oceanward outflow branch (MacCready et al., 2018; Wang et al., 2017). The material transport and mixing associated with estuarine exchange flow is of critical importance for salinity dynamics, and also biogeochemistry in the estuary (MacCready & Geyer, 2024; Wang et al., 2017).

Writing – original draft: Dongxiao Yin
Writing – review & editing: Dongxiao Yin, Courtney K. Harris, John C. Warner

Estuarine exchange flow is the primary driver that determines the salt balance in the estuary as river discharges typically transport zero salinity. The variations of estuarine exchange flow at different timescales (e.g., spring-neap, meteorological bands, seasonal, and annual) can lead to significant changes in salt transport and the salt content of the estuaries (Banas et al., 2004; Bowen & Geyer, 2003; Chen & Sanford, 2009; Lerczak et al., 2006; MacCready & Geyer, 2024; Rayson et al., 2017; Scully et al., 2005; Xie & Li, 2018). Understanding the physical mechanisms behind such variations are of significant importance considering the influence of estuarine salinity on water quality, aquaculture, and ecosystem function of the estuary and its adjacent wetlands (Fagherazzi et al., 2019; Getz & Eckert, 2023; Tully et al., 2019). Additionally, estuarine exchange flow plays a pivotal role in regulating the biogeochemistry in the estuary (MacCready & Geyer, 2024). On one hand, the fact that the magnitude of the estuarine exchange flow is usually many times larger than the river discharge means it dictates the flushing of the estuary and the residence time of the waterborne materials within the estuary (Du et al., 2018; MacCready & Geyer, 2010; Xiong et al., 2021). On the other hand, exchange flow exerts control on the import, redistribution, and export of biologically important materials, including nitrogen and dissolved oxygen (Olson et al., 2020; Sutton et al., 2013; Xiong et al., 2024), making it a key factor in regulating all aspects of biogeochemical processes in estuaries. Thus, studying estuarine exchange flow is crucial for understanding both the physical and biogeochemical processes in estuaries.

Estuarine exchange flow is subject to the control of various external forcings including winds, tides, and river discharge. These forcings vary at different timescales, resulting in changes in estuarine exchange flow. At the meteorological band (timescales of several days), both remote and local winds affect estuarine exchange flow. The remote wind imposes a subtidal water level component at the mouth of the estuary (Cook et al., 2023; Feng & Li, 2010; Garvine, 1985; Huang & Li, 2017; Wang, 1979; Xu et al., 2008), while local winds influence the surface slope in the estuary and modulate its salinity structure (Barlow, 1956; Feng & Li, 2010; Garvine, 1985; Geyer, 1997; Li et al., 2018). The impact of wind on estuarine exchange flow is related to wind direction and intensity (Gong et al., 2009). Moderate local down-estuary axial winds can increase subtidal shear dispersion in an estuary, causing enhanced volume and salt transport due to estuarine exchange flow, and resulting in increased salt content in the estuary (Chen & Sanford, 2009; Scully et al., 2005; Xie & Li, 2018). On the other hand, intense local winds in either the up-estuary or down-estuary axial direction tend to destroy the vertical stratification in an estuary, reducing the volume and salt transport due to estuarine exchange flow, leading to a decrease in the estuary's salt content (Chen & Sanford, 2009; Scully et al., 2005; Xie & Li, 2018). Additionally, cross-estuary local wind-induced lateral circulation can further complicate the effects of axial wind on estuarine exchange flow and associated salt transport (Li & Li, 2011, 2012; Xie & Li, 2018).

Estuarine exchange flow often shows variation at the spring-neap timescale. Tidal currents generally serve as the source of mixing in an estuary and can vary significantly during the spring-neap cycle (Jay & Smith, 1990a, 1990b). For estuarine exchange flow that is primarily driven by baroclinic pressure gradients (i.e., gravitational circulation), stronger tides can reduce stratification and decrease the estuarine exchange flow (Geyer et al., 2020; Park & Kuo, 1996). For instance, in the Hudson River estuary, estuarine exchange flow and the associated landward salt transport is much higher during the neap tides than during the spring tides. This difference results in factor-of-4 variations in the salt content in the Hudson River estuary during a spring-neap cycle (Bowen & Geyer, 2003; Lerczak et al., 2006). On the other hand, for estuarine exchange flow driven by tidal currents, salt transport mainly results from the temporal correlation between current velocity and salinity (i.e., tidal oscillatory salt flux, Fischer et al., 1979; see also Geyer & Signell, 1992; Lerczak et al., 2006), and is found to be larger during stronger tides (Banas et al., 2004; Chen et al., 2012).

At seasonal and annual timescales, estuarine exchange flow varies with seasonal and interannual variations in river discharge. In Chesapeake Bay, interannual variations of estuarine exchange flow are attributed to changes in river discharge (Xiong et al., 2021). The annual cycle of dry summers and wet winters are reported to be responsible for the intra- and interannual variation of estuarine exchange flow over a seasonally inverse estuary (Nidzieko & Monismith, 2013). In Coos estuary, Oregon, the varying river discharge at seasonal timescale causes the change in the oceanward component of the estuarine exchange flow but has little influence on its landward counterpart (Conroy et al., 2020).

Current understanding of estuarine exchange flow is primarily based on studies of estuaries where tidal influence is significant (e.g., Fischer et al., 1979; Hansen & Rattray, 1965; MacCready & Geyer, 2024), with a focus on coastal plain estuaries such as Chesapeake Bay and the Hudson River estuary (as reviewed in MacCready &

Geyer, 2010). In contrast, there is limited understanding of how estuarine exchange flow behaves in systems where tidal forcing is negligible. In addition, fewer studies have examined coastal lagoons, despite their widespread presence along global coastlines and their critical role as productive coastal ecosystems (Knoppers, 1994). Moreover, most research on coastal lagoons has focused on the exchange between the lagoon and the coastal ocean through inlets (e.g., Sylaios et al., 2006; Valle-Levinson et al., 2001), with limited understanding of internal exchange between sub-basins within the lagoon. However, many coastal lagoons have multiple sub-basins or tributary estuaries. This is particularly true of large lagoons, such as the Albemarle-Pamlico estuarine system (APES), the largest coastal lagoon estuary in the U.S. (Paerl et al., 2010). This study aims to address this gap by investigating the mechanisms controlling estuarine exchange flow in the APES, a representative example of large lagoonal estuaries with weak tides, multiple tidal inlets, and several tributary estuaries/sub-basins.

1.2. Study Area and Motivation

The APES (Figure 1) is located on the northeast coast of North Carolina, U.S. In terms of surface area, it is the second largest estuary on the U.S. East Coast, covering an area of ~7,800 km^2. It is a shallow estuary with a mean water depth of 4.5 m. The APES is isolated from the Atlantic Ocean by the North Carolina Outer Banks barrier island chain. Exchange between the ocean and the APES occurs through three major inlets including Ocracoke Inlet, Hatteras Inlet, and Oregon Inlet. The tidal range is 0.9 m on average along the barrier island oceanic coastline (Moslow & Heron, 1994) but is damped to 0.1 m or less over most of the APES region (Wells & Kim, 1989). Consequently, similar to many coastal lagoon systems isolated from the open ocean by barrier islands, tides play a negligible role in controlling circulation in most parts of the APES that are far from the inlets (Wells & Kim, 1989). The APES contains two major sub-basins, Albemarle Sound to the north and Pamlico Sound to the south. There are four major rivers entering the APES. The Chowan and Roanoke Rivers empty into Albemarle Sound while the Pamlico and Neuse Rivers drain into Pamlico Sound. River discharges are high during spring and low during summer with an annual load of 29×10^9 m^3 (Jia & Li, 2012a; Lin et al., 2007). The response of the salinity in the APES to river discharge is not instantaneous. Based on 18 years observation, on average, December is the month of highest salinity although the minimum flow occurs in June or October (Epperly & Ross, 1986; Giese et al., 1985).

At timescales of several days, the estuarine circulation in the APES is driven mainly by wind but shows a spatially distinct pattern and dynamics (Luettich Jr et al., 2002, see also Pietrafesa, Janowitz, Chao, et al., 1986; Pietrafesa, Janowitz, Miller, et al., 1986; Wells & Kim, 1989). In specific, circulation in southern Pamlico Sound (west of Bluff Shoal, Figure 1b) often features vertically sheared two-layer flows that is driven primarily by wind stress, baroclinic, and barotropic forces. However, in northern Pamlico Sound (east of Bluff Shoal, Figure 1b) and in Albemarle Sound, the circulation shows laterally sheared flows that is driven primarily by wind stress and barotropic forces (Jia & Li, 2012b). On annual average, Pamlico Sound features a weakly stratified two-layer circulation while Albemarle Sound is generally well mixed (Jia & Li, 2012a; Woods, 1967). The gravitational force is the main driver of the long-term mean circulation in Pamlico Sound (Jia & Li, 2012a). Tides, although being negligible in most parts of the APES (Luettich Jr et al., 2002), generate strong currents around the inlets and are an important factor controlling exchange between the APES and the open ocean (Clunies et al., 2017; Jia & Li, 2012a; Mulligan et al., 2019; Wells & Kim, 1989).

The exchange between the APES and the Atlantic Ocean through the inlets is characterized by two distinct modes (stratified or well-mixed) depending partially on wind directions (Xie & Eggleston, 1999; Xie & Pietrafesa, 1999). The subtidal salt fluxes at the inlets are controlled by subtidal barotropic advection and tidal oscillatory salt transport (Jia & Li, 2012a). Jia and Li (2012a) considered a transect in southern Pamlico Sound and reported that the annual mean exchange flow driven by gravitational circulation can reach 2 cm/s there. There is also evidence that the salt content of the APES changes monthly and seasonally (Jia & Li, 2012a; Lin et al., 2007; Wells & Kim, 1989). The salt content tends to be lower from late winter to spring and higher from late summer to early winter. Lowest and highest salinities are reported to occur in April and December, respectively (Epperly & Ross, 1986).

The APES and its tributary estuaries have been historically challenged by environmental issues including harmful algal blooms (e.g., Paerl, 1982; Paerl, 1997) and bottom water hypoxia (e.g., Buzzelli et al., 2002; Stanley & Nixon, 1992). The development of harmful algal blooms and low-oxygen bottom water have been primarily related to the increased nutrient delivery from upland through the river discharge and its subsequent accumulation

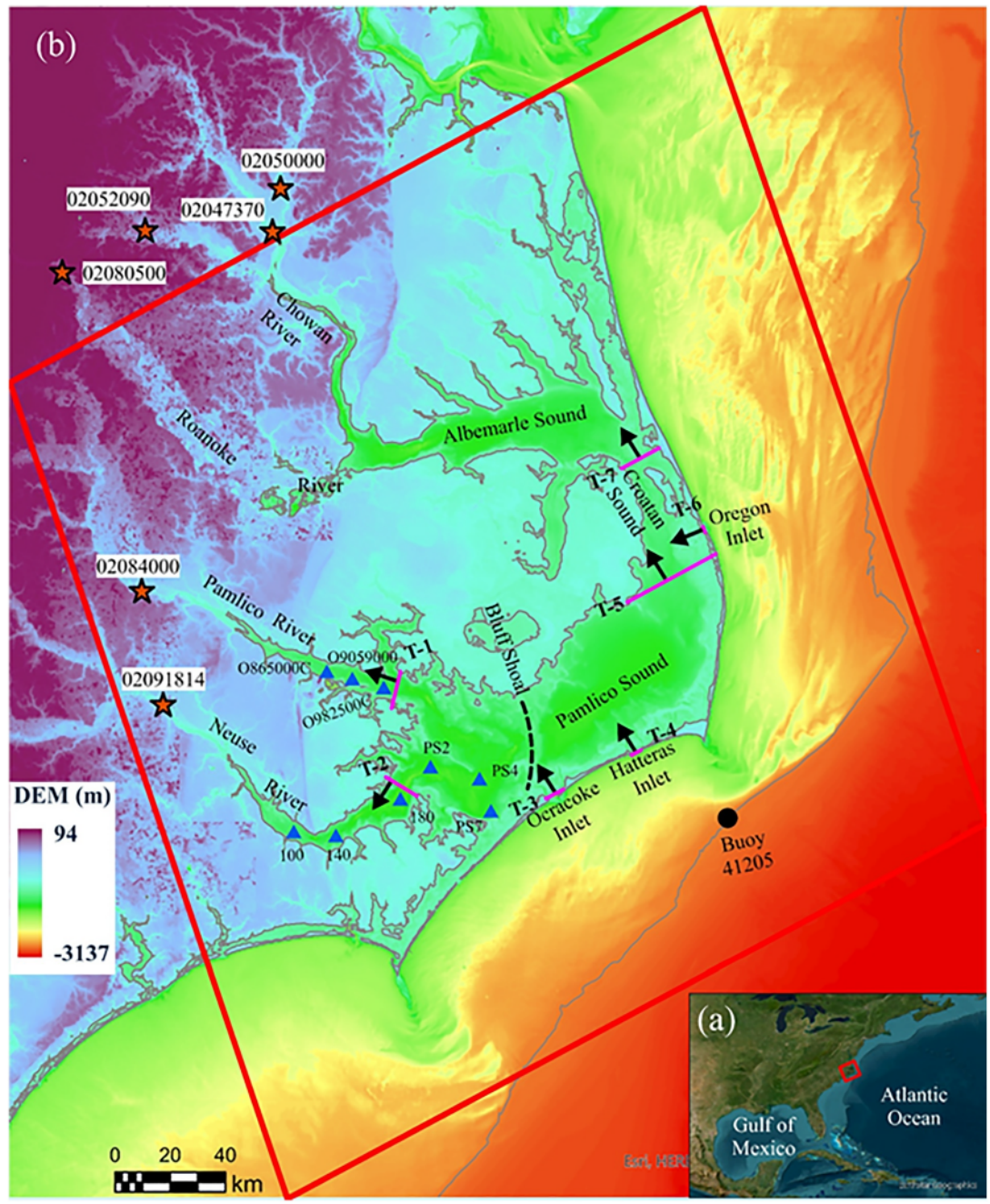

Figure 1. (a) Location of the study area within the Atlantic Ocean, (b) the Albemarle-Pamlico estuarine system and the adjacent coastal region. The red box outlines the model domain. The stars represent USGS gauge stations of observed hourly river discharge. Blue triangles identify locations of salinity data. The pink lines show the locations of the transects where total exchange flow analysis was conducted. The black arrows at each transect point to the directions defined as inward volume transport. Dark gray lines depict the 0-m and 50-m isobaths. The black dashed line indicates the location of Bluff Shoal, which divides Pamlico Sound into northern and southern parts. The location of Buoy 41205 used in Figure 2b is also shown.

in the system largely due to the long residence time of the APES (e.g., Paerl et al., 2010; Paerl et al., 2014; Paerl et al., 2018; Pietrafesa, Janowitz, Chao, et al., 1986; Pietrafesa, Janowitz, Miller, et al., 1986). Yet the role of estuarine exchange flow in regulating estuarine biogeochemistry and these issues has been overlooked.

Basic understanding of the estuarine exchange flow in the APES remains unclear. For instance, what is the magnitude of estuarine exchange flow within the APES and within its sub-basins? What are the major

mechanisms controlling estuarine exchange flow? How do estuarine exchange flow and associated salt transport vary at different timescales? And how may the salt content of the estuary respond to the variation in estuarine exchange flow? What is the potential role of estuarine exchange flow in regulating the biogeochemical processes? These questions motivated this study.

1.3. Theoretical Background

1.3.1. Total Exchange Flow

In this study, we use the total exchange flow (TEF) analysis framework to quantify the estuarine exchange flow and associated salt transport (MacCready, 2011). TEF tracks the subtidal volume and salt transport in salinity coordinates (MacCready, 2011). It represents the estuarine exchange flow and associated salt transport as occurring in two layers with inward volume transport (Q_{in}, in m^3/s) and volume weighted salinity (S_{in}, in psu), and outward volume transport (Q_{out}, in m^3/s) and volume weighted salinity (S_{out}, in psu). In comparison to the Eulerian decomposition method, TEF allows a concise quantification of the estuarine exchange flow, which exactly satisfies the Knudsen relations, and separate considerations of the contributions of volume transport (Q_{in} and Q_{out}) and salinity (S_{in} and S_{out}) to salt transport (MacCready & Geyer, 2024).

Using the TEF volume transport terms (Q_{in} and Q_{out}), considering river discharge (Q_R, in m^3/s), the volume conservation of the estuary can be expressed as follows:

$$\frac{d}{dt}\left\langle \int d_V \right\rangle = Q_{in} + Q_{out} + Q_R \tag{1}$$

where $\langle\rangle$ represents a tidal average, Q_{in} is the inward (positive) volume transport, Q_{out} is the outward (negative) volume transport, and Q_R is the river discharge (positive).

Using the TEF volume transport (Q_{in} and Q_{out}) and the salinity terms (S_{in} and S_{out}), the salt balance of the estuary can be written as follows:

$$\frac{d}{dt}\left\langle \int s d_V \right\rangle = \frac{d\overline{SV}}{dt} = \frac{d\overline{S}}{dt}\overline{V} + \frac{d\overline{V}}{dt}\overline{S} = F_{net} = Q_{in}S_{in} + Q_{out}S_{out} = Q_{in}\Delta S - Q_R S_{out} + \frac{d\overline{V}}{dt}S_{out} \tag{2}$$

where $\overline{V} = \langle \int d_V \rangle$ (unit: m^3) is the tidally averaged volume of the estuary and $\overline{S} = \left\langle \frac{\int s d_V}{\int d_V} \right\rangle$ (unit: psu) is the salt content of the estuary, which is calculated as the tidally and volume averaged salinity of the estuary. $\Delta S = S_{in} - S_{out}$ is the salinity difference between inward and outward volume transport-weighted salinities. In Equation 2, the contributions of volume transport (Q_{in} and Q_{out}) and associated salinities (S_{in} and S_{out}) on estuarine salt budget are considered separately.

Combining Equations 1 and 2, the salt balance equation can be further written as follows:

$$\frac{d}{dt}\left\langle \int s d_V \right\rangle - \frac{d}{dt}\left\langle \int d_V \right\rangle * S_{out} = Q_{in}\Delta S - Q_R S_{out} \tag{3}$$

The left-hand side of this equation is the adjusted storage term (MacCready & Geyer, 2024), which is related to the estuarine adjustment time as described below.

1.3.2. Estuarine Adjustment Time

Estuarine adjustment time refers to the timescale needed for an estuary to adapt from an original steady state to a new steady state following a change in external forcings (Hetland & Geyer, 2004; Kranenburg, 1986; MacCready, 1999, 2007). Depending on the relative length of the estuarine adjustment time and the timescale at which the forcings vary, the estuarine response can be quasi-steady or unsteady (MacCready, 2007). In this study, we analyze the response of the salt content (represented using $\overline{S} = \left\langle \frac{\int s d_V}{\int d_V} \right\rangle$) to variations in estuarine exchange flow and associated salt transport in the APES. Here, we define the estuarine adjustment time as the time needed for the

salt content of the estuary to reach a new steady state following changes in estuarine exchange flow and associated salt transport. Two timescales at which the estuarine exchange flow varies are considered—a relatively short unsteady timescale and a relatively long quasi-steady timescale. As shown in Section 3, the unsteady timescale at which the estuarine exchange flow of the APES varies includes the meteorological band (several days) and the spring-neap cycle (~2 weeks). Because our analysis considers tidally averaged values, the unsteady timescale covers subtidal frequencies up to the spring-neap cycle. It is defined as unsteady as both the meteorological band and the spring-neap cycle are generally shorter than the estuarine adjustment time of the APES. The quasi-steady timescale is represented using the annual means of the estuarine properties such as TEF terms and salt content. It is defined as quasi-steady because it is generally longer than the estuarine adjustment time of the APES. At the annual average timescale, the estuary is adjusted to the fluctuations in estuarine exchange flow and associated salt transport, and Equations 1 and 3 can be further simplified as follows:

$$0 = Q_{\text{in}} + Q_{\text{out}} + Q_R \tag{4}$$

$$\frac{d}{dt}\left\langle \int s d_V \right\rangle = \frac{d\overline{S}}{dt}\overline{V} = Q_{\text{in}}\Delta S - Q_R S_{\text{out}} \tag{5}$$

However, at the spring-neap cycle and meteorological bands, the system is in a nonsteady state condition, and $\frac{d}{dt}\langle \int d_V \rangle$ in Equations 1 and 3 cannot be neglected (MacCready & Geyer, 2024).

1.3.3. Physical Mechanisms Related to Estuarine Exchange Flow

A significant amount of work has been conducted to understand the physical mechanisms controlling estuarine exchange flow and to build theoretical or empirical relationships between estuarine exchange flow and external forcing (MacCready & Geyer, 2010; see also Burchard & Hetland, 2010; Chatwin, 1976; Hansen & Rattray, 1965; Hetland & Geyer, 2004; MacCready, 1999, 2004, 2007, MacCready & Geyer, 2024; Monismith et al., 2002; Ralston et al., 2008). Estuarine exchange flow can be induced by residual shear (i.e., the variations of the tidally averaged velocity and salinity) and/or tidal currents themselves (MacCready & Geyer, 2024). Numerous studies have been conducted to develop theoretical solutions for residual shear induced estuarine exchange flow and associated estuarine stratification (Burchard & Hetland, 2010; Hansen & Rattray, 1965; MacCready, 2004, 2007; Ralston et al., 2008). For estuaries in which exchange flow are forced by the tidal advection and flow separation, Chen et al. (2012) and MacCready and Geyer (2024) investigated the scaling between estuarine exchange flow and tidal forcing. In this study, we use the solutions for subtidal shear velocity and salinity deviation from Ralston et al. (2008), and scaling from Chen et al. (2012) and MacCready and Geyer (2024) as the theoretical guidelines to understand the physical controls behind the estuarine exchange flow in the APES.

For a residual circulation-dominated estuary, based on the solution of subtidal shear velocity from Ralston et al. (2008); see also Burchard & Hetland (2010); the estuarine exchange flow (represented using Q_{in}) scales with the residual shear velocity as follows:

$$Q_{\text{in}} \propto u\,A = \left(\alpha_u\, u_0 + \beta_u\, u_E + \gamma_u\, u_w\right)A \tag{6}$$

where A (unit: m^2) is the area of a selected cross-section, and u (unit: m/s) is the subtidal shear velocity, which can be separated into the exchange flow velocity components induced by barotropic flow (u_0), gravitational circulation (u_E), and local along-estuary wind (u_w). In addition, α_u, β_u and γ_u are functions of the normalized depth ($\frac{z}{H}$), which range from 0 to -1 where H (unit: m) is the water depth.

At the short unsteady timescale, based on the solutions of u_0, u_E, and u_w (Ralston et al., 2008), depending on the controlling mechanisms, it is expected that (a) $Q_{\text{in}} \propto \frac{\partial \eta}{\partial t}$ when estuarine exchange flow is affected primarily by $\frac{\partial \eta}{\partial t}$, (b) $Q_{\text{in}} \propto \frac{\partial S_0}{\partial x}/(K_m)$ when estuarine exchange flow is affected primarily by gravitational circulation, and (c) $Q_{\text{in}} \propto \frac{\tau_w}{K_m} \propto \frac{V_w^2}{K_m}$ when estuarine exchange flow is affected primarily by wind-induced straining. Here, η (unit: m) is the subtidal water level, $\frac{\partial \eta}{\partial t}$ (unit: m/s) represents the temporal change of the subtidal water level associated with

Table 1
Short Unsteady Timescale Scaling Expectations for Estuarine Exchange Flow and Associated Salinity Difference

Timescale	Controlling mechanism	Scaling (Q_{in})	Scaling (ΔS)
Short unsteady	$\frac{\partial \eta}{\partial t}$	$Q_{\text{in}} \propto \frac{\partial \eta}{\partial t}$	$\Delta S \propto \frac{1}{K_s}\left(\frac{\partial S_0}{\partial x}\right)\frac{\partial \eta}{\partial t}$
	u_E	$Q_{\text{in}} \propto \frac{\partial S_0}{\partial x}/(K_m)$	$\Delta S \propto \left(\frac{\partial S_0}{\partial x}\right)^2/(K_m K_s)$
	Wind-induced straining	$Q_{\text{in}} \propto \frac{\tau_w}{K_m} \propto \frac{V_a^2}{K_m}$	$\Delta S \propto \frac{1}{K_s}\left(\frac{\partial S_0}{\partial x}\right) V_a^2$
	Current-salinity tidal correlation	$Q_{\text{in}} \propto Q_{\text{prism}}$	$\Delta S \propto \frac{1}{Q_{\text{prism}}}$

Note. For estuarine exchange flow dominated by residual shear, the scaling for ΔS applies when tidally averaged flows have two layers in vertical, with the top layer going seaward and the bottom layer going landward.

winds, s_0 (unit: psu) represents depth-averaged salinity, K_m (unit: m^2/s) is the eddy viscosity, and τ_w (unit: N/m^2) and V_a (unit: m/s) are the wind stress and wind velocity, respectively.

In estuaries featuring vertically two-layered residual circulation (e.g., Pritchard, 1952), the volume transport-averaged salinity difference (represented using ΔS in Equation 2) will follow the following scaling:

$$\Delta S \propto s' = \frac{H^2}{K_s}\left(\frac{\partial S_0}{\partial x}\right)\left(\alpha_s * u_0 + \beta_s * u_E + \gamma_s * u_w\right) \tag{7}$$

where s' (psu) is the salinity deviation from the depth-averaged salinity (s_0) (Ralston et al., 2008). Additionally, α_s, β_s and γ_s are functions of the normalized depth ($\frac{z}{H}$), and K_s (unit: m^2/s) is the eddy diffusivity coefficient, which is proportional to K_m by a constant (MacCready and Geyer).

Thus, for estuaries where the tidally averaged flows have two layers, with the top layer going seaward and the bottom layer going landward, the following scalings between ΔS and the controlling factors are expected: (a) $\Delta S \propto \frac{1}{K_s}\left(\frac{\partial S_0}{\partial x}\right)\frac{\partial \eta}{\partial t}$, when estuarine exchange flow is affected primarily by $\frac{\partial \eta}{\partial t}$; (b) $\Delta S \propto \left(\frac{\partial S_0}{\partial x}\right)^2/(K_m K_s)$ when estuarine exchange flow is affected primarily by gravitational circulation; and (c) $\Delta S \propto \frac{1}{K_s}\left(\frac{\partial S_0}{\partial x}\right) V_a^2$ when estuarine exchange flow is affected primarily by wind-induced straining.

For exchange flow that is forced by the oscillating tidal motion and flow separation (i.e., current-salinity tidal correlation), according to Chen et al. (2012), we may expect that Q_{in} scales with the tidal prism (Q_{prism}, in m^3/s), that is, $Q_{\text{in}} \propto Q_{\text{prism}} = \frac{1}{T}\int_0^{T/2} A U_T \sin(\omega t)\, dt$, where T (unit: s) is the tidal period and U_T (unit: m/s) is the magnitude of tidal velocity (Chen et al., 2012). In addition, ΔS is expected to decrease with increased tidal prism, that is, $\Delta S \propto \frac{1}{Q_{\text{prism}}}$ (MacCready & Geyer, 2024). It should be noted that, under high subtidal barotropic flow ($\alpha_u\, u_0\, A$ in Equation 6) conditions, Q_{prism} should be corrected by removing the subtidal barotropic flow from the tidal volume flux.

Table 1 summarizes the expected scaling of the estuarine exchange flow (Q_{in}) and associated salinity difference (ΔS) at short unsteady timescale when controlled by different mechanisms.

The scalings are shown in Table 1 for idealized estuaries with simplified geometry, external forcing, physical processes, and steady state assumptions, but for a realistic estuary, at short unsteady timescale, the general expectations will be as follows: (a) Q_{in} and ΔS vary with $\frac{\partial \eta}{\partial t}$, for cases where the time rate of change of residual water level is the major driver of the estuarine exchange flow; (b) Q_{in} and ΔS increase with increases in the horizontal salinity gradient ($\frac{\partial S_0}{\partial x}$), and decreases in mixing (K_m,K_s) for gravitational circulation induced exchange flow; (c) when estuarine exchange flow is controlled by wind-induced straining (instead of direct mixing), we may expect Q_{in} and ΔS to increase with V_a^2 as the wind-induced straining tends to suppress the mixing (K_m) (Chen & Sanford, 2009; Scully et al., 2005); and (d) for estuarine exchange flow forced by tidal correlation between currents and salinity, it is expected that Q_{in} increases while ΔS decreases with increased tidal forcing.

Table 2
Long Quasi-Steady Timescale Scaling Expectations for Estuarine Exchange Flow and Associated Salinity Difference

Timescale	Controlling mechanism	Scaling (Q_{in})	Scaling (ΔS)
Long quasi-steady	River discharge-induced barotropic flow.	$Q_{in} \propto k\, Q_R$	$\Delta S \propto k\, Q_R$
	River discharge-enhanced gravitational circulation.	$Q_{in} \propto Q_R^n$	$\Delta S \propto Q_R^n$

At a long quasi-steady timescale, we focused on the impact of river discharge because the net influence from winds and tides on residual circulation in the APES tends to approach zero at long timescales, and the river discharge becomes the dominating factor (Wells & Kim, 1989). The effect of river discharge on estuarine exchange flow can be executed through two ways: (a) forming an oceanward barotropic gradient thus increasing the seaward barotropic flow (u_0 in Equation 6 and Equation 7) and (b) enhancing the estuarine exchange flow induced by gravitational circulation (u_e in Equation 6 and Equation 7) by modifying salinity structure and stratification. At the quasi-steady timescale, the horizontal salinity gradient ($\frac{\partial S_0}{\partial x}$ in Equation 7), which scales with K_m, should have fully adjusted to the scale of river discharge (MacCready & Geyer, 2010; see also MacCready, 1999, 2004, 2007). Thus, if the control of river discharge on the estuarine exchange flow is mainly via barotropic effects, it is expected that the estuarine exchange flow and salinity difference at a long quasi-steady timescale will scale linearly with river discharge according to Equations 6 and 7. However, if the impact of river discharge on estuarine exchange flow and salinity difference is mainly via gravitational circulation, then the estuarine exchange flow and salinity difference will scale with river discharge as power-law functions, that is, $Q_{in} \propto Q_R^n$ and $\Delta S \propto Q_R^n$ (e.g., MacCready & Geyer, 2010; Monismith et al., 2002; Ralston et al., 2008). The expected scaling of the estuarine exchange flow (Q_{in}) and associated salinity difference (ΔS) at long quasi-steady timescale is summarized in Table 2.

1.4. Objective and Research Questions

In this study, we aim to understand the estuarine exchange flow, net salt transport associated with exchange flow and its impact on salt content and implications for biogeochemistry in the APES. We focused our analysis on the short unsteady and long quasi-steady timescales defined above. Particularly, we answer the following four research questions: (a) What are the magnitudes of estuarine exchange flow (represented using Q_{in} in Equation 1) and net salt transport (represented using F_{net} in Equation 2) in the APES, and how do they vary at both the unsteady and quasi-steady timescales? (b) What are the physical controls on the estuarine exchange flow in the APES? (c) How does the salt content (represented using $\overline{S} = \left\langle \frac{\int s d_V}{\int d_V} \right\rangle$ in Equation 2) in the estuary respond to variations in estuarine exchange flow at both the unsteady and quasi-steady timescales? (d) What are the biogeochemical implications of estuarine exchange flow? To address the research questions, we developed a three-dimensional hydrodynamic model using the Regional Ocean Modeling System (ROMS; see Haidvogel et al., 2000, 2008; Shchepetkin & McWilliams, 2003, 2009) within the Coupled Ocean-Atmosphere-Wave-Sediment Transport (COAWST) model framework (see Warner et al., 2008, 2010). We applied the TEF method to quantify estuarine exchange flow and salt transport.

To understand the physical mechanisms controlling estuarine exchange flow at the short unsteady timescale, we conducted a wavelet power analysis to identify the dominant timescales of estuarine exchange flow variability at the inlets of the APES, its sub-basins, and tributary estuaries. By comparing the power spectra of estuarine exchange flow with those of external forcings, we identified potential drivers that may influence exchange flow. Next, we examined the scaling relationship between estuarine exchange flow and potential forcing(s), comparing our results with theoretically derived scalings (Table 1) to identify the major dynamical mechanisms. It should be noted that our goal in analyzing these scaling relationships at short unsteady timescale focuses on identifying a significant trend between estuarine exchange flow and the external forcing that align with theoretical scaling relations summarized in Table 1. We do not expect a perfect fit because the scaling relationships are based on idealized systems, whereas the modeled results include the complex geometry and nonsteady forcing of the APES.

To understand the controlling mechanism over long quasi-steady timescales, we conducted a scaling analysis to examine the correlation between estuarine exchange flow and river discharge, specifically evaluating whether it

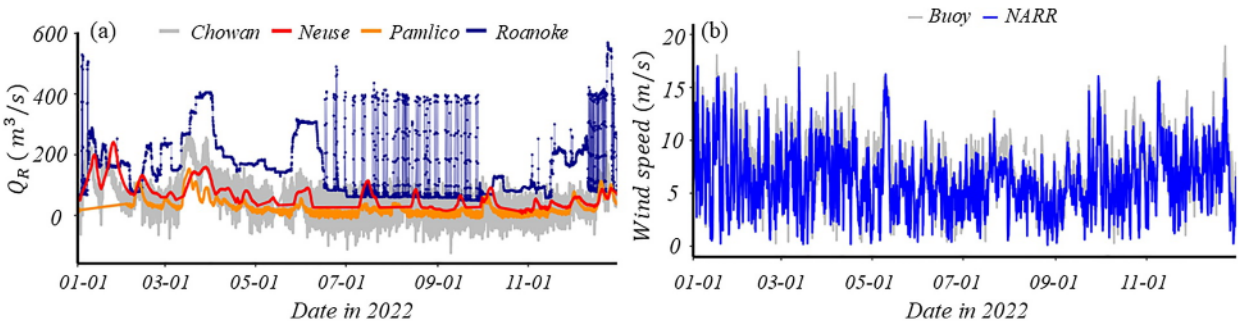

Figure 2. (a) Hourly time series of observed river discharges during 2022 for the Chowan (gray), Neuse (red), Pamlico (orange), and Roanoke (dark blue) Rivers. (b) 3-hourly time series of wind speed from North American Regional Reanalysis used as our model input (blue) along with hourly wind observation (gray) at Buoy 41205 during 2022. The locations of the USGS gauging stations and Buoy 41205 are shown in Figure 1b.

follows a linear or power-law relationship. This analysis enables us to identify the major mechanism by comparing the observed relationship with theoretical expectations, as summarized in Table 2.

The biogeochemical implications of estuarine exchange flow are discussed in terms of its role in controlling the flushing efficiency of the APES and regulating the exchange of biologically important materials between the APES and the coastal ocean, as well as among its sub-basins.

In Section 2, we present the configuration of the numerical model, the setup of the numerical experiments, and the calculations of estuarine exchange flow. Results of model-simulated salinity, salt content, calculated estuarine exchange flow, and wavelet analysis are presented in Section 3. In Section 4, we discuss the controlling mechanisms behind estuarine exchange flow and the salt content response to variations of estuarine exchange flow at both the short unsteady and long quasi-steady timescales. In addition, we discuss the implications of estuarine exchange flow for estuarine biogeochemistry. In Section 5, we close the paper with Summary and Conclusions.

2. Methods

2.1. Numerical Model Configuration and Validation

The Regional Ocean Modeling System (ROMS) is used to represent the hydrodynamics of the APES. ROMS is a free-surface, hydrostatic, and primitive equation model that has been widely used in numerical investigations of estuarine systems (e.g., Geyer et al., 2020; Sutherland et al., 2011; Warner et al., 2005). Our model domain (red box in Figure 1b) encompasses the entire APES and extends ~40 km offshore of the North Carolina Outer Banks barrier islands. The model has a horizontal resolution of ~500 m and 16 terrain-following stretched sigma coordinate layers. The $k-\varepsilon$ method of the generic length scale turbulence closure formulation (Umlauf & Burchard, 2003) is used. The default third-order upstream advection scheme and fourth-order, centered differences scheme is used for horizontal and vertical momentum, respectively. For tracers, the third high order spatial interpolation at the middle temporal level coupled with a TVD limiter (HSIMT, Wu & Zhu, 2010) is used.

Model initial and boundary conditions including temperature, salinity, water level, and three-dimensional momentum are derived from a lower resolution "parent" ROMS 3D model that covers the entire U.S. East Coast with a horizontal resolution of ~5 km (Warner & Kalra, 2022). River inputs for our APES ROMS model are derived from the U.S. Geological Survey (USGS) gauge stations. Specifically, hourly river discharge time series (Figure 2a) for the Neuse River, Pamlico River, and Roanoke River are taken from USGS gauging stations 02091814, 02084000, and 02080500 (see Figure 1b for locations), respectively. Note that the high-frequency fluctuations in Roanoke River discharge are caused by human alterations to streamflow via dam openings and closings. For the Chowan River (Figure 2a), the river discharge time series used in the model is the combination of the observations from the three most downstream USGS gauging stations including 02052090, 02047370, and 02050000 (see Figure 1b for locations). Discharges measured at the gauge stations represent runoff from the catchments upstream of the gauge stations, but areas downstream of the stations also contribute freshwater to the estuaries. To account for surface runoff from these ungauged areas, the discharges measured at the gauge stations are scaled by the ratio between the ungauged and gauged area. The temperature for the river discharge are set as

Table 3
Correlation Metrics Comparing Modeled and Observed Values of Salinity in the Surface and Bottom Waters of Nine Observation Sites

		Surface values			Bottom values		
Region	Station	RMSE (psu)	Bias (psu)	R^2	RMSE (psu)	Bias (psu)	R^2
Neuse River estuary	100	2.21	−0.47	0.64	1.92	−0.49	0.63
	140	1.61	1.25	0.86	1.86	0.54	0.61
	180	1.54	1.15	0.84	1.95	0.87	0.64
Pamlico River estuary	O865000C	1.47	−0.53	0.88	2.80	−0.68	0.35
	O9059000	2.88	2.39	0.73	2.05	0.82	0.60
	O982500C	2.35	1.26	0.74	2.50	1.36	0.55
Pamlico Sound	PS2	1.37	1.2	0.92	1.62	1.00	0.81
	PS4	1.87	1.59	0.87	2.25	0.81	0.48
	PS7	1.66	1.26	0.87	2.46	1.78	0.82

10°C. Atmospheric forcings for the simulation are from the 3-hourly North American Regional Reanalysis (NARR, Mesinger et al., 2006), which is produced by the National Centers for Environmental Prediction and has a horizontal resolution of 32 km. The atmospheric forcing is interpolated to match the spatial and temporal resolutions of the APES ROMS model. At each time step, the spatially varying atmospheric forcing is applied to compute the surface boundary conditions. Figure 2b compares the NARR winds with observations at Buoy 41025 (see Figure 1b for buoy location). Overall, the NARR winds well reproduce the observed wind speed ($R^2 = 0.74$).

Because the "parent" ROMS model does not account for freshwater input into the APES, the salinity in the model domain is initialized as follows. The model is first initialized with oceanic salinity and run from February 2021 to September 2022 including freshwater input. Model output from September 2022 is then used as the initial condition to rerun the model from September 2021 until December 2022. Following this initialization procedure, the model output from the year 2022 is used for analysis in this study. Based on annual mean river discharge observations from 2000 to 2023, year 2022 is the driest year for the past decade (Figure S1a in Supporting Information S1) and is among the 25% driest years in the past two decades (Figure S1b in Supporting Information S1). The baroclinic time step used for the model simulation is 30 s, and the number of barotropic time steps between each baroclinic time step is 20. Output files are written once per hour.

The numerical model is validated with surface and bottom salinity measurements in Pamlico River, Neuse River, and Pamlico Sound (see Figure 1b for locations of salinity observation sites). The salinity measurements in Pamlico River estuary (stations O865000C, O9059000, and O982500C), Neuse River estuary (stations 100, 140, and 180), and Pamlico Sound (stations PS2, PS4, and PS7) are acquired by the North Carolina Environmental Quality's Ambient Monitoring System, the Neuse River Estuary Modeling and Monitoring Project (ModMon), and the Ferry Monitoring program (FerryMon, Paerl et al., 2009), respectively. The metrics used for model performance evaluation are the root mean square error (RMSE), the averaged bias (Bias), and the correlation coefficient (R^2). See the (Equations S1–S3 in Supporting Information S1) for details of the calculation of the metrics. Table 3 shows the correlation metrics for model simulation of surface and bottom salinity at these nine stations. Figure 3 compares the simulated and the observed surface and bottom salinity at three selected stations (model-data comparison at the other six stations is shown in Figure S2 in Supporting Information S1). The model in general captured both the magnitude and spatial-temporal variation of the salinity in the APES, despite some discrepancies at certain sites and time points. The lower model performance in Figure 3d is largely due to the underestimation of the peak salinity value in May 2022, which might be due to the limitation in representing the local bathymetry. For Figure 3f, the bias maybe primarily induced by the boundary conditions.

2.2. Numerical Experiments: Sensitivity to River Discharge

In addition to the numerical simulation driven by realistic forcing for 2022 described above, we conduct three additional numerical simulations with varying river discharges to examine the influence of river discharge on estuarine exchange flow and associated salt transport at the quasi-steady timescale. Table 4 details the

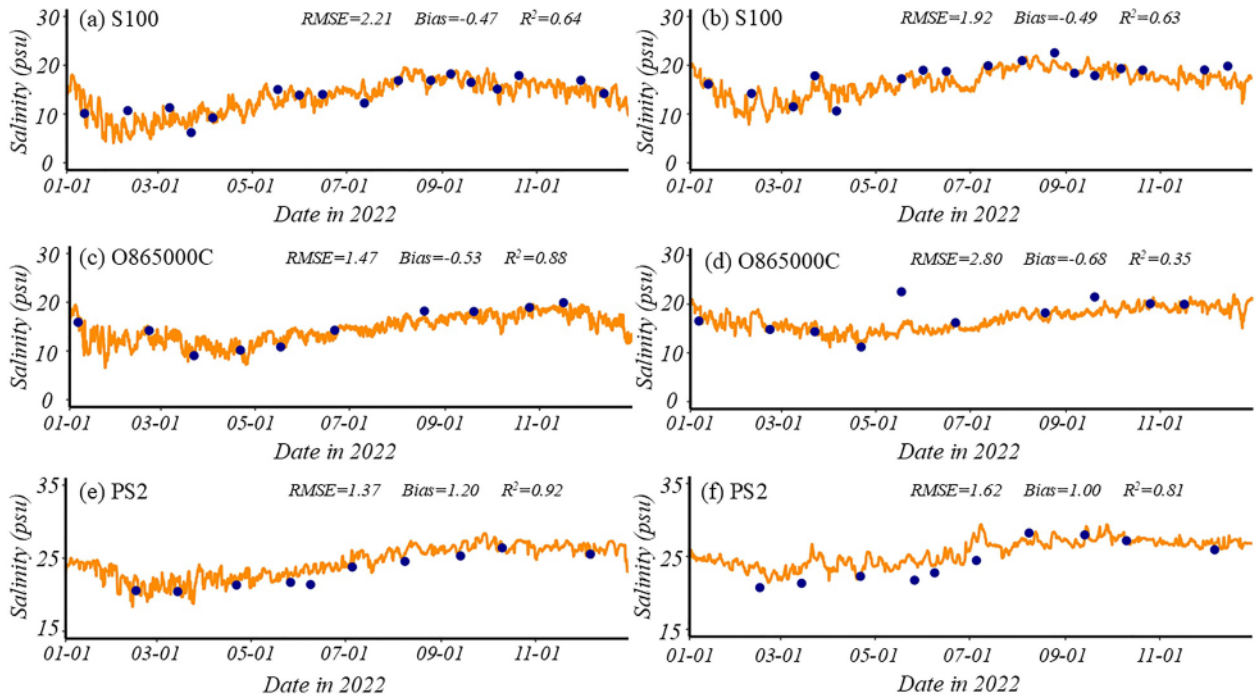

Figure 3. *Left*: observed (blue circles) and modeled (orange lines) surface salinity at three selected stations from the Pamlico River estuary (S100), Neuse River estuary (O86500C), and Pamlico Sound (PS2) during 2022. *Right*: same as the left panel, but for bottom salinity. Correlation metrics (root mean square error, Bias and R^2) are also shown. The locations of the stations are shown in Figure 1b.

configuration of these numerical experiments, which were all identical except for the scaling of the river discharge. We focus on river discharge because the net influence from winds and tides on residual circulation in the APES tends to approach zero at long timescales, and the river discharge becomes the dominating factor (Wells & Kim, 1989). In each run, the river discharge is scaled by a factor ranging from 0.1 to 2.0. The ranges of river discharge are chosen to provide clear scaling between the river input and the estuarine exchange flow as shown in Section 4.

2.3. Estuarine Exchange Flow Calculations

In this study, following the TEF method (MacCready, 2011), we calculate the subtidal inward (Q_{in}) and outward (Q_{out}) volume transport and subtidal inward (S_{in}) and outward (S_{out}) volume transport-weighted salinities through six transects in the APES (Figure 1b). Hourly model outputs (i.e., hourly history files from ROMS) for the year 2022 are used for the calculation. The TEF method requires binning the salt transport through a given transect by salinity. In our calculations, we use 100 salinity bins ranging from 0 to 36. The first step in TEF calculations for a transect is to compute the volume flux of water with salinity exceeding each salinity value. A Butterworth low-pass filter with a 35-hr cutoff frequency is then applied to these volume fluxes to extract their subtidal components. The subtidal volume flux within each salinity bin is determined as the difference between the subtidal volume fluxes of water with salinities exceeding the lower and upper bounds of the bin. The subtidal salt flux within each bin is calculated as the product of the corresponding volume flux and salinity. Using these results, subtidal inward (Q_{in}) and outward (Q_{out}) volume transports, as well as inward (F_{in}) and outward (F_{out}) salt transports, are calculated by integrating the respective volume and salt fluxes over the salinity bins. The transport-weighted subtidal inward (S_{in}) and outward (S_{out}) salinities are then computed as F_{in}/Q_{in} and F_{out}/Q_{out}, respectively.

With the calculated TEF terms, the estuarine adjustment time of salt content to change in exchange flow is calculated following Rayson et al. (2017) as follow:

Table 4
The Configuration of the Numerical Experiments

Experiment	River discharge	Wind	Tide
Standard	Realistic forcing for 2022		
River 1	0.1 × Standard	Realistic forcing for 2022	
River 2	0.5 × Standard	Realistic forcing for 2022	
River 3	2.0 × Standard	Realistic forcing for 2022	

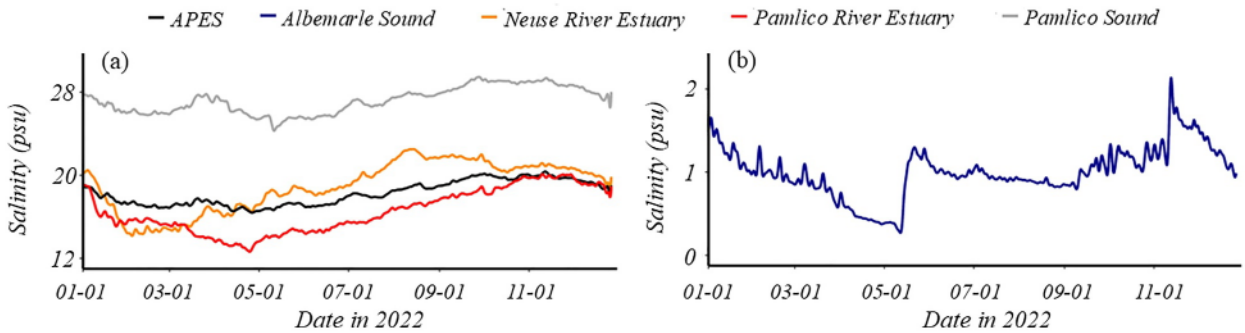

Figure 4. (a) Time series of salt content of the Albemarle-Pamlico estuarine system (black), Pamlico Sound (gray), Pamlico River estuary (red), and Neuse River estuary (orange) during 2022 and (b) same as (a) but for Albemarle Sound (blue). These values are calculated from the results for the year 2022 from the "Standard" model (Table 4).

$$T_{adj} = \frac{\Sigma}{\left|\frac{d\Sigma}{dt}\right|} \tag{8}$$

where $\Sigma = \frac{\overline{S}}{S_{in}}$ and $\overline{S} = \left\langle \frac{\int s dv}{\int dv} \right\rangle$, which represents the salt content of the estuary.

For the rest of the paper, we present the estuarine exchange flow, and the associated salt transport calculated at the transects shown in Figure 1b from the results of the year 2022 from the numerical model runs (Table 4). Additionally, we discuss the physical mechanisms that control the estuarine exchange flow at both the short unsteady (i.e., subtidal to spring-neap) and long quasi-steady (i.e., annual average) timescales using the theoretical scalings that are reviewed in Section 1.3. Moreover, we examine the responses of the salt content of the APES and its sub-basins to the variations of the estuarine exchange flow at these two timescales and interpret such responses with respect to the calculated estuarine adjustment time. Further, we discuss the implications of estuarine exchange flow to biogeochemistry in the APES.

3. Results

3.1. Salt Content

Figure 4 shows the time series of the salt content ($\overline{S}$ in Equation 2) of the APES and its sub-basins during the year 2022. The salt content of Albemarle Sound (shown in a separate panel Figure 4b) is much lower than the APES and the other sub-basins (Figure 4a). Over the entire year, Albermarle Sound salt content only varies from 0 to ~2.0 psu. Meanwhile, Pamlico (red line in Figure 4a) and Neuse River (orange line in Figure 4a) estuaries vary from ~13.0 to ~23.0 psu, Pamlico Sound (gray line in Figure 4a) varies from ~24.0 to ~29.0 psu, and the APES (black line in Figure 4a) varies from ~16.0 to 20.0 psu. Seasonally, salt content of the APES increases from 16.5 to 20.0 psu over a period of ~5 months. The salt content slightly decreases and then stays relatively stable before a seasonal drop lasting from late fall in November to late winter in February. From then until late spring, the salt content of the APES stays relatively stable except for a slight increase and then decrease occurring over a one-and-a-half-month period starting from March. These three distinct time periods in general characterize Pamlico Sound (gray line), Pamlico River (red line), and Neuse River (orange line) estuaries aside from some short-term differences (Figure 4a). For example, the salt content of Pamlico River estuary shows a constant drop from March to May while the APES, Pamlico Sound, and Neuse River estuary all exhibit an increase and then a decrease. On the other hand, the salt content of Albemarle Sound stays relatively stable during summer and early fall before decreasing from late fall in November to spring.

3.2. Salinity and Stratification

Figure 5a shows the annual mean surface salinity based on the results of the "Standard" model (Table 4) for the year 2022. As with previous observational (Pietrafesa, Janowitz, Chao, et al., 1986; Pietrafesa, Janowitz, Miller, et al., 1986; Wells & Kim, 1989) and modeling studies (Jia & Li, 2012a; Lin et al., 2007), annual mean salinities are essentially fresh in Albemarle Sound but have estuarine values in Pamlico Sound and much of Pamlico River

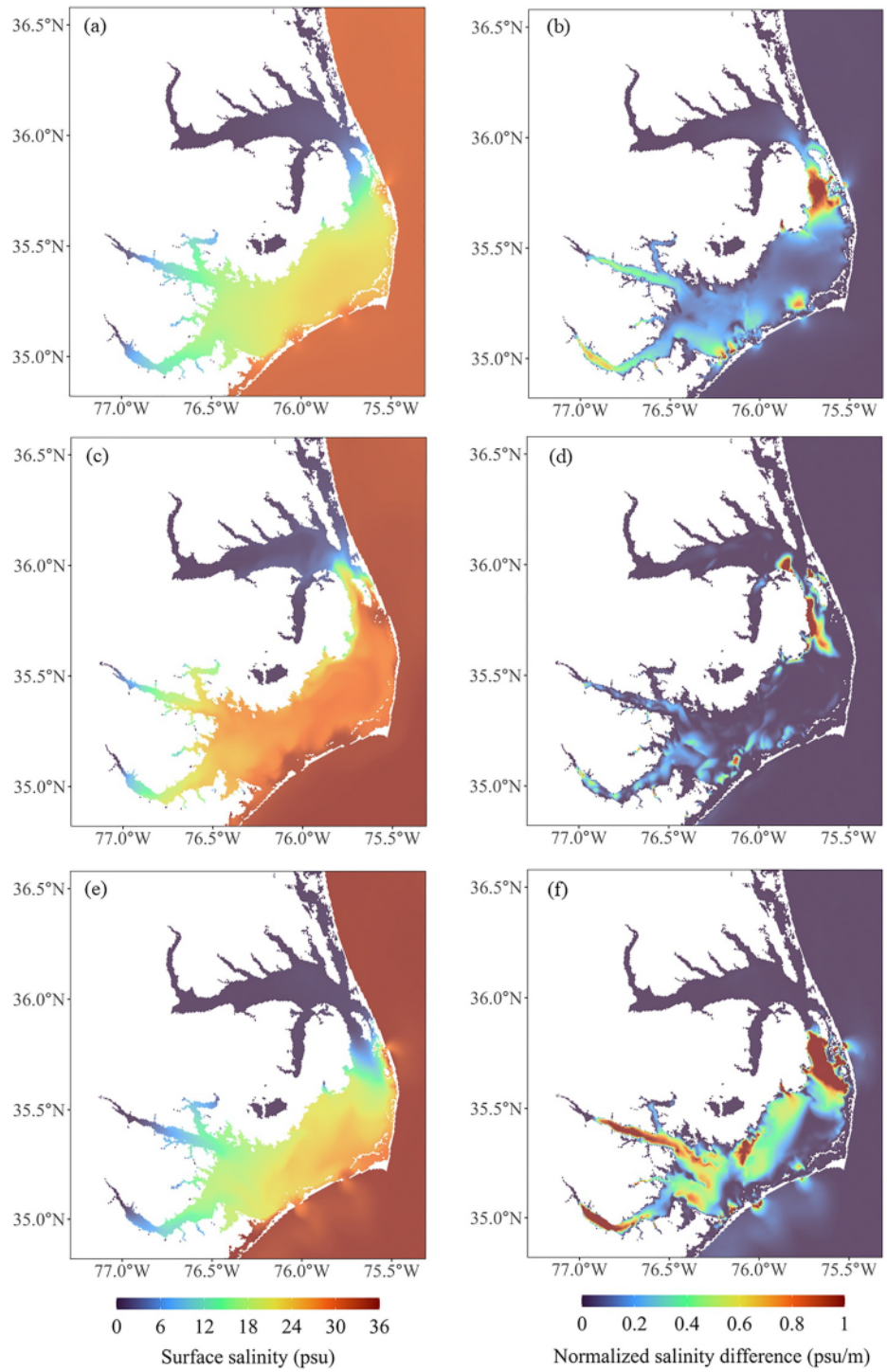

Figure 5. *Top*: the distribution of annual mean (a) surface salinity and (b) bottom-to-surface salinity difference normalized by water depth over the Albemarle-Pamlico estuarine system (APES) and the adjacent coastal regions. *Middle*: same as the top, but for the daily mean salinity on 12 November 2022, when the salt content of the APES is at its maximum (Figure 4a). *Bottom*: same as the top, but for the daily mean salinity on 26 April 2022, when the salt content of the APES is at its minimum (Figure 4a). These values are calculated from the results of the year 2022 from the "Standard" model (Table 4).

and Neuse River estuaries (Figure 5a). Aside from Pamlico River and Neuse River estuaries as well as Croatan Sound (the inlet between Albemarle and Pamlico Sounds, Figure 1b), the depth normalized annual mean bottom-surface salinity difference (Figure 5b) of APES is minimal, indicating its overall weak stratification.

Figures 5c and 5e show the daily mean salinity when the salt content of the APES are at its maximum and minimum for the year 2022 (Figure 4a), respectively. When salt content of the APES is at its maximum of the year (Figure 5c), compared to the annual-averaged condition (Figure 5a), salinity is much higher over Pamlico Sound, and high salinity water intrude from Pamlico Sound further into Albemarle Sound and the tributary estuaries. On the other hand, when salt content of the APES is at its minimum of the year (Figure 5e), salinity appears to be lower at the mouth of Albemarle Sound and tributary estuaries with low-salinity water entering Pamlico Sound from Albemarle Sound and tributary estuaries. This increase/decrease of salinity over Pamlico Sound along with the intrusion/retreat of salt water plume into/out of Albemarle Sound and tributary estuaries indicates the control of seasonally varied river discharge on salinity of the system as also reported by previous studies (e.g., Epperly & Ross, 1986).

Figures 5d and 5f show the daily mean bottom-surface salinity difference normalized by water depth on days when the salt content of the APES are at its maximum and minimum of the year 2022 (Figure 4a), respectively. Overall, in comparison to the annual-averaged condition (Figure 5b), depth normalized bottom-surface salinity difference over the APES is decreased when its salt content is at its maximum of the year (Figure 5e); however, bottom-surface salinity difference is increased when salt content of the APES is at its minimum of the year (Figure 5f). This indicates high water column stratification during the wet season and low stratification during the dry season, controlled by river discharge.

3.3. Estuarine Exchange Flow and Its Temporal Variation

3.3.1. Pamlico River and Neuse River Estuaries

Figures 6a and 6b show the calculated TEF terms (Q_{in}, Q_{out}, S_{in} and S_{out}) for Pamlico River estuary (transect 1 in Figure 1b). Visual inspection of the time series of subtidal volume transports (Figure 6a) and salinities (Figure 6b) indicates their variations at timescales of several days. The wavelet power spectra for Q_{in} and ΔS are presented in Figures 6c and 6d, respectively. Both figures indicate episodic, dominating and recurrent energy at periods in the range of 3–8 days. High wavelet power levels are also found at periods of 8–20 and ~90 days but with a much less frequent occurrence. Averaging the wavelet power spectra over time in Figures 6c and 6d, we obtain the averaged wavelet power spectra as shown in Figures 6e and 6f. Both plots identify a peak wavelet power at the period of ~6 days, which aligns with the wavelet power spectra of the wind speed (Figure S3a in Supporting Information S1). This indicates that the dominating forcing behind such short-term variations of the exchange flow and associated salinity difference is wind. Furthermore, the wavelet power spectra (Figures 6c and 6d) show no detectable spring-neap signal, indicating that tides play a negligible role in the tributary estuaries, which is consistent with the region's small tidal range. The estuarine exchange flow and associated salinity calculated for the Neuse River estuary transect (transect 2 in Figure 1b) exhibit a temporal trend similar to those for the Pamlico River estuary transect (Neuse River estuary transect data shown in Figures S3b and S4 in Supporting Information S1).

3.3.2. Ocracoke, Hatteras, and Oregon Inlets

Figures 7a and 7b show the calculated TEF terms (Q_{in}, Q_{out}, S_{in} and S_{out}) at the Ocracoke Inlet transect (transect 3 in Figure 1b). Their corresponding power spectra are shown in Figures 7c and 7d, respectively. The figures of power spectra indicate that the wavelet power mainly concentrates at two periods: 2–8 and ~16 days. The averaged wavelet power spectra of Q_{in} (Figure 7e) and ΔS (Figure 7f) identify peak wavelet power with periods at the spring-neap cycle (peaks at ~15 days in Figures 7e and 7f) and within the meteorological band (peaks at ~4 and ~6 days in Figures 7e and 7f). The peak at the spring-neap cycle suggests the control of tidal forcing while the peaks falling within the meteorological band indicates the strong influence of the barotropic flow. These analyses are also conducted for the Hatteras Inlet and the Oregon Inlet (transects 4 and 6 in Figure 1b) with similar results (Figures S5 and S6 in Supporting Information S1).

3.3.3. Albemarle Sound

Figures 8a and 8b show the calculated TEF terms (Q_{in}, Q_{out}, S_{in}, and S_{out}) at Albemarle Sound (transect 7 in Figure 1b). Visual inspection of the time series indicates their variations at timescales of several days. The power

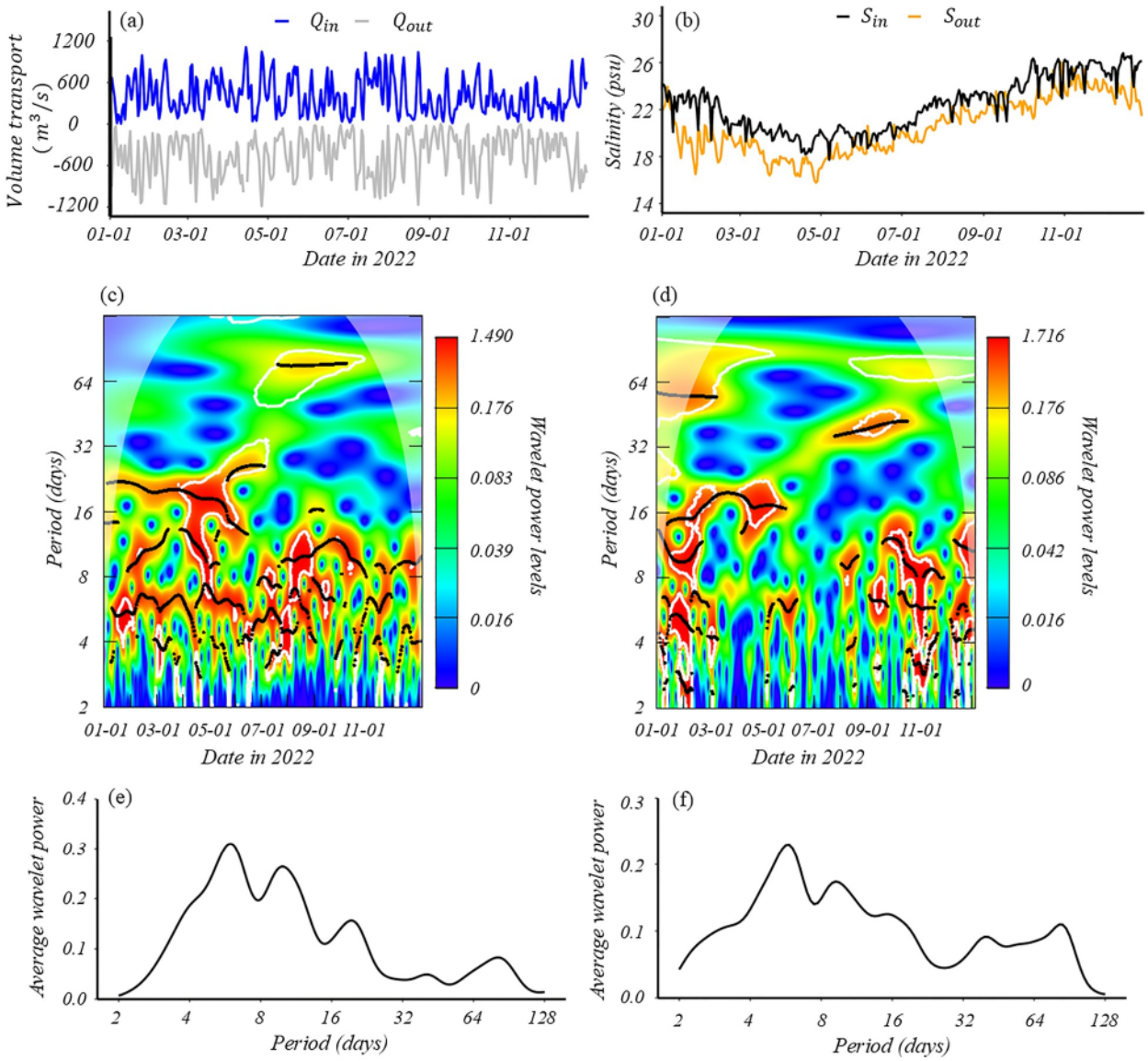

Figure 6. *Top*: time series of (a) Q_{in} (blue) and Q_{out} (gray) and (b) S_{in} (black) and S_{out} (orange) at Pamlico River estuary transect during 2022. *Middle*: wavelet power spectrum of (c) Q_{in} and (d) ΔS. The black lines identify the dominant periodicities. *Bottom*: averaged wavelet power of (e) Q_{in} and (f) ΔS. The location of the Pamlico River estuary transect and the defined direction of inward volume transport are shown at Transect 1 in Figure 1b.

spectra for Q_{in} and ΔS are presented in Figures 8c and 8d, respectively. Both figures indicate episodic, dominating and recurrent energy at periods in the range of 3–10 days. High wavelet power levels are also found at periods of ~16 days but occurs much less frequently. Figures 8e and 8f identify a peak wavelet power at the period of 4–6 days, indicating the control of meteorological forcing on estuarine exchange flow and associated salinity.

3.4. Annual Mean Estuarine Exchange Flow From "Standard" Model

As described in Section 1.3.2, we use the annual average as indicative of the quasi-steady response. Figure 9a shows the annual-averaged Q_{in} (blue) and Q_{out} (gray) along with the annual mean river discharge that drains into the APES and its sub-basins. Overall, the volume transport of estuarine exchange flow is larger than the river inputs. Assuming steady state condition, we can calculate the river amplification factor α_R as $\alpha_R = \frac{Q_{in}}{Q_R}$ (MacCready, 2011; Sutherland et al., 2011). Based on results from the "Standard" model for the year 2022, α_R are 3.6, 9.1 and 7.6 for the APES, the Neuse River estuary, and the Pamlico River estuary, respectively. These values generally fall within the range of a partially mixed estuary ($2 < \alpha_R < 34$, MacCready & Geyer, 2010), such as

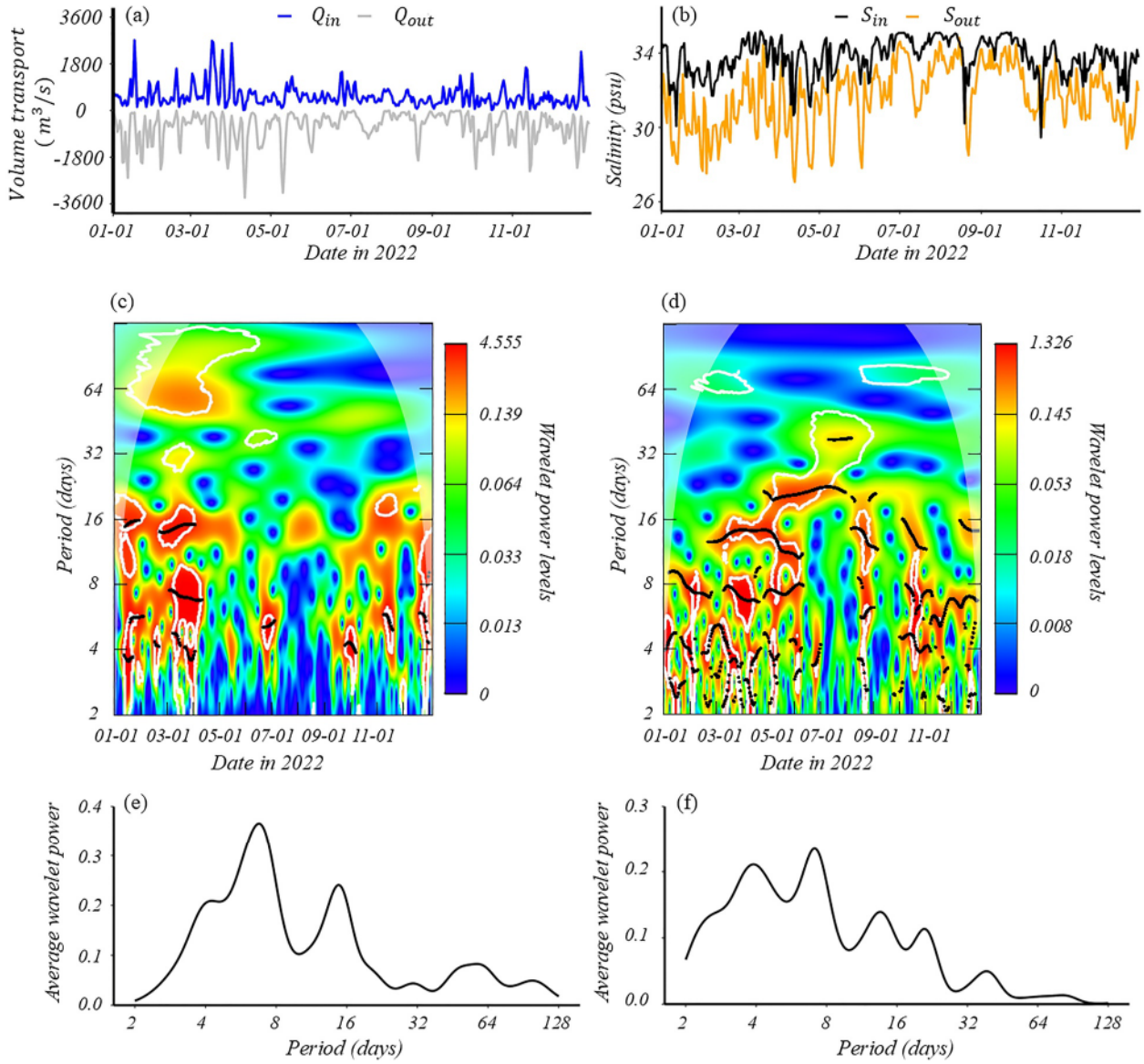

Figure 7. *Top*: time series of (a) Q_{in} (blue) and Q_{out} (gray) and (b) S_{in} (black) and S_{out} (orange) at the Ocracoke Inlet transect during 2022. *Middle*: wavelet power spectrum of (c) Q_{in} and (d) ΔS. The black lines identify the dominant periodicities. *Bottom*: averaged wavelet power of (e) Q_{in} and (f) ΔS. The location and the defined direction of inward volume transport are shown at Transect 3 in Figure 1b.

Chesapeake Bay (α_R = 1.5–4, Xiong et al., 2021) and the Hudson River (α_R = 2.5, Chen et al., 2012). This indicates their partially mixed nature at steady state, consistent with previous research that classified these systems as partially mixed on long timescales (Jia & Li, 2012a). However, α_R for Albemarle Sound is only 1.3, which is attributed to its weak estuarine circulation. This is likely associated with its shallow water depth, low salinity values, and a low horizontal salinity gradient at the mouth of the sound. Estuaries with similar characteristics, such as weak residual circulation and shallow water depths, also exhibit α_R values of around 1; examples include Mobile Bay (Du et al., 2018), the Merrimack River (Chen et al., 2012), and the Columbia River (MacCready, 2011).

Figure 9b illustrates the range and spatial variability of the annual-averaged S_{in} (black) and S_{out} (orange). The transport-weighted salinity imported from the open ocean to the APES through the three major inlets (Hatteras, Ocracoke, and Oregon inlets) ranges from 32.5 to 34.6. The salinity then decreases as it transports to other parts of the APES, indicating mixing processes and the addition of freshwater. The largest modification to the salinity

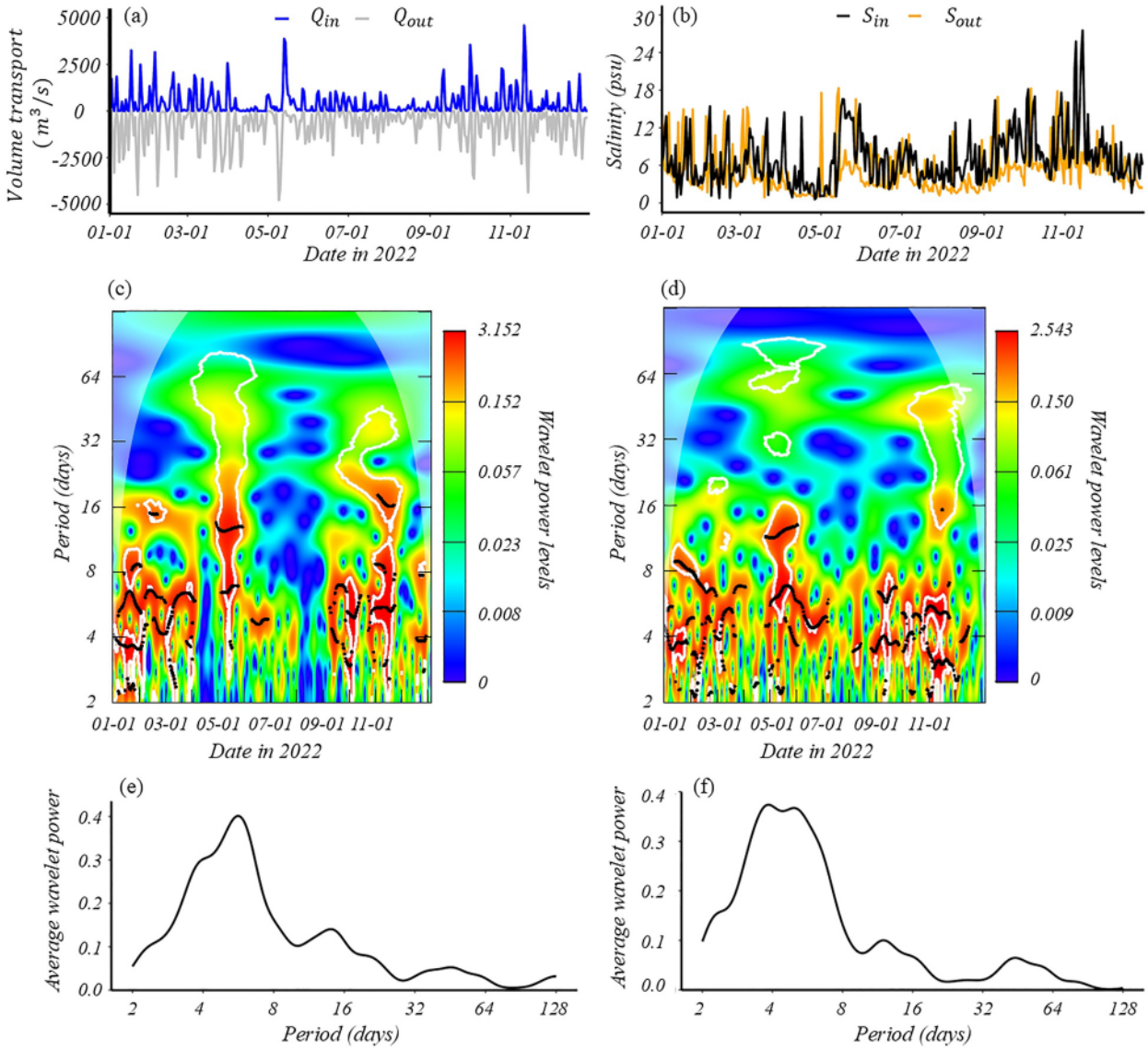

Figure 8. *Top*: time series of (a) Q_{in} (blue) and Q_{out} (gray) and (b) S_{in} (black) and S_{out} (orange) at the Albemarle Sound transect during 2022. *Middle*: wavelet power spectrum of (c) Q_{in} and (d) ΔS. The black lines identify the dominant periodicities. *Bottom*: averaged wavelet power of (e) Q_{in} and (f) ΔS. The location and the defined direction of inward volume transport are shown at Transect 7 in Figure 1b.

occurs between Albemarle Sound, Pamlico Sound, and the Oregon Inlet. For instance, S_{in} imported from the open ocean through the Oregon Inlet is 32.5 and that from Pamlico Sound is 24.4 (transects 5 and 6 in Figure 1b). However, the salinity import S_{in} decreases to 7.0 over the mouth of Albemarle Sound (transect 7 in Figure 1b). This sharp reduction indicates the limited intrusion of salt waters from Pamlico Sound and coastal ocean into Albemarle Sound, which is due to the rapidly decreased water depth from the Pamlico Sound transect (transect 5 in Figure 1b) to the Albemarle Sound transect (transect 7 in Figure 1b).

4. Discussion

4.1. Unsteady Timescale: Controlling Mechanisms and Salt Content Response

In this section, the estuarine exchange flow, salt transport, and salt content response are analyzed for the short unsteady timescale, defined here as timescales that encompass the meteorological band and the spring-neap cycle (see Section 1.3.2). The system response is unsteady at these timescales because they are shorter than estuarine adjustment time (MacCready, 2007).

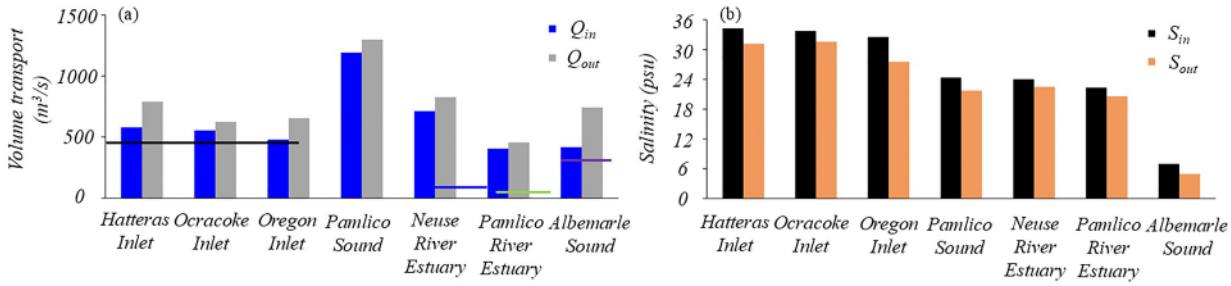

Figure 9. Annual-averaged (a) Q_{in} (blue) and Q_{out} (gray) and (b) S_{in} (black) and S_{out} (orange) at the Hatteras Inlet (transect 4), Ocracoke Inlet (transect 3), Oregon Inlet (transect 6), Pamlico Sound (transect 5), Neuse River estuary (transect 2), Pamlico River estuary (transect 1), and Albemarle Sound (transect 7). For reference, the horizontal black, blue, green, and purple lines in (a) represent the annual-averaged river discharge into the Albemarle-Pamlico Estuarine System, Neuse River estuary, Pamlico River estuary, and Albemarle Sound, respectively. These total exchange flow terms are calculated from the results of the year 2022 from the "Standard" model (Table 4). The river discharges are calculated from the USGS observations shown in Figure 2a. The locations of the transects and the defined directions of inward volume transport are shown in Figure 1b.

4.1.1. Tributary Estuaries: The Role of Wind Straining

The influence of wind on estuarine exchange flow is analyzed by examining the potential scaling relations of Q_{in} and ΔS with the along-estuary wind stress at the Pamlico River estuary. Based on the wavelet power spectra of wind (Figure S3 in Supporting Information S1), we calculate the along-estuary wind speed averaged over the dominant timescale of the meteorological band (~6 days) using a Butterworth low-pass filter with a cutoff frequency of 8 days (Figure 10a). Based on wind direction, 15 down-estuary wind periods (red) and 13 up-estuary wind periods (blue) are identified for the year 2022. Wind stress for each wind period is represented using the square of along-estuary wind speed (V_a^2) and is plotted against Q_{in} (Figure 10b), ΔS (Figure 10c), $Q_{\text{in}} * \Delta S$ (Figure 10d) and F_{net} (Figure 10e). All terms shown in Figures 10b–10d are wind period-averaged for each down-estuary and up-estuary wind period. Both volume transport Q_{in} (Figure 10b) and salinity difference ΔS (Figure 10c) exhibit a significant increasing trend (p-values <0.05, positive slope) with V_a^2. As a result, the salt transport ($Q_{\text{in}} * \Delta S$) due to estuarine exchange flow also increases with increased wind stress (Figure 10c). These significant trends are consistent with the expected scaling when estuarine exchange flow is dominated by wind-induced straining (Table 1), as has been reported in previous studies (Chen & Sanford, 2009; Scully et al., 2005). Further analysis (not shown) indicates insignificant trend between Q_{in} and $\frac{\partial S_0}{\partial x}$, and a significant increasing trend between ΔS and $\frac{\partial S_0}{\partial x}$ with an R^2 of 0.18, which is much less than that for ΔS and V_a^2 ($R^2 = 0.37$). These analyses suggest that wind-induced straining plays a significant role in driving estuarine exchange flow and associated salt transport over Pamlico River estuary. However, it should be noted that the net salt flux F_{net} (Figure 10e) decreases with increased V_a^2 though $Q_{\text{in}} * \Delta S$ increases with it. This is due to salinity loss from the decrease in the volume of the estuary (i.e., $\frac{d\overline{V}}{dt} S_{\text{out}}$ in Equation 2) when more water is flushed out of the estuary with higher down-estuary wind stress. It should be noted that scaling of current-salinity tidal correlation is not tested for the tributary estuaries due to the negligible influence of tides, as evidenced by the extremely small tidal range (less than 0.1 m) and the absence of a spring-neap signal in the wavelet power spectra (Figures 6c and 6d). Similar results are also found over Neuse River estuary (Figure S4 in Supporting Information S1), confirming the significant role of wind-induced straining on estuarine exchange flow and associated salt transport over the two tributary estuaries of the APES at the short unsteady timescale.

4.1.2. Inlets: The Role of Tidal Prism (Q_{prism}) and Residual Water Level Variation ($\frac{\partial \eta}{\partial t}$)

To explore the major mechanisms that influence estuarine exchange flow at the inlets, the calculated TEF terms shown in Figure 7 is decomposed into two parts using a Butterworth low-pass filter with a cutoff frequency of 8-day. The low-pass filtered components ($Q_{\text{in\_SN}}$ and ΔS_{SN}) have frequencies longer than 8 days while the residual component ($Q_{\text{in\_residual}}$ and $\Delta S_{\text{residual}}$) have frequencies less than 8 days. We test the scaling relationships between the low-pass filtered components ($Q_{\text{in\_SN}}$ and ΔS_{SN}) and the tidal prism ($Q_{\text{prism\_SN}}$), as well as between the residual components ($Q_{\text{in\_residual}}$ and $\Delta S_{\text{residual}}$) and $\frac{\partial \eta}{\partial t}$ (Figures 11b–11d and 12b–12d). The goal of these scaling analyses is to evaluate whether statistically significant (i.e., p-value less than 0.05), decreasing (negative slope) or

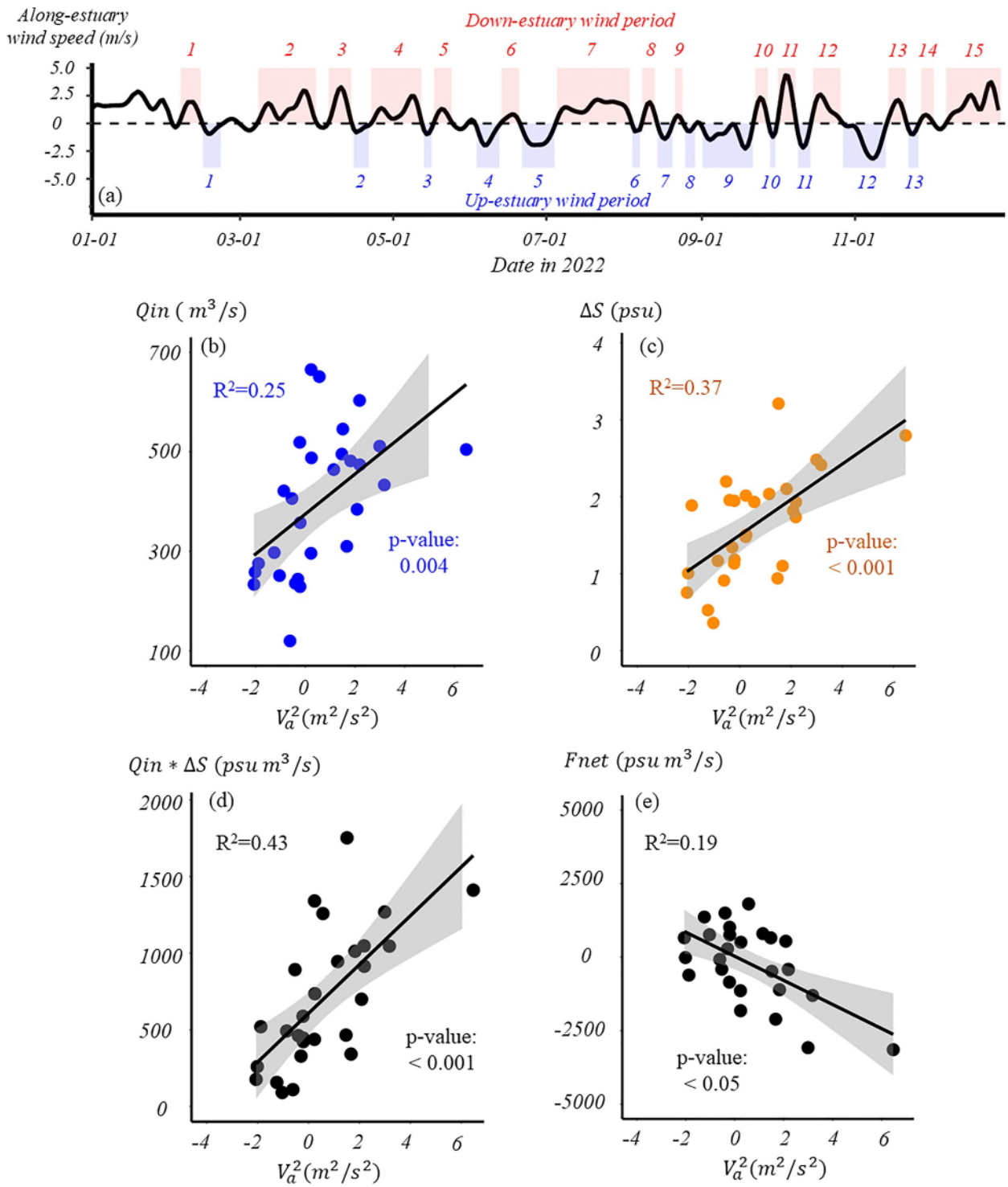

Figure 10. *Top*: time series of (a) along-estuary wind speed at the Pamlico River estuary transect during 2022. The wind data are from North American Regional Reanalysis and is low-pass filtered with a cutoff frequency of 8 days. Wind speeds >0 are blowing down-estuary; <0 are blowing up-estuary. Panel (a) identifies the 15 down-estuary wind period (red) and the 13 up-estuary wind period (blue). *Middle and bottom*: the square of the wind period-averaged along-estuary wind speed (V_a^2) versus (b) Q_{in}, (c) ΔS, (d) $Q_{in} * \Delta S$, and (e) F_{net} at the Pamlico River estuary transect. The linear regression lines and the p-values are also shown. Total exchange flow terms are calculated from the results of the year 2022 from the "Standard" model (Table 4). The location of the Pamlico River estuary transect, and the defined direction of inward volume transport are shown at Transect 1 in Figure 1b.

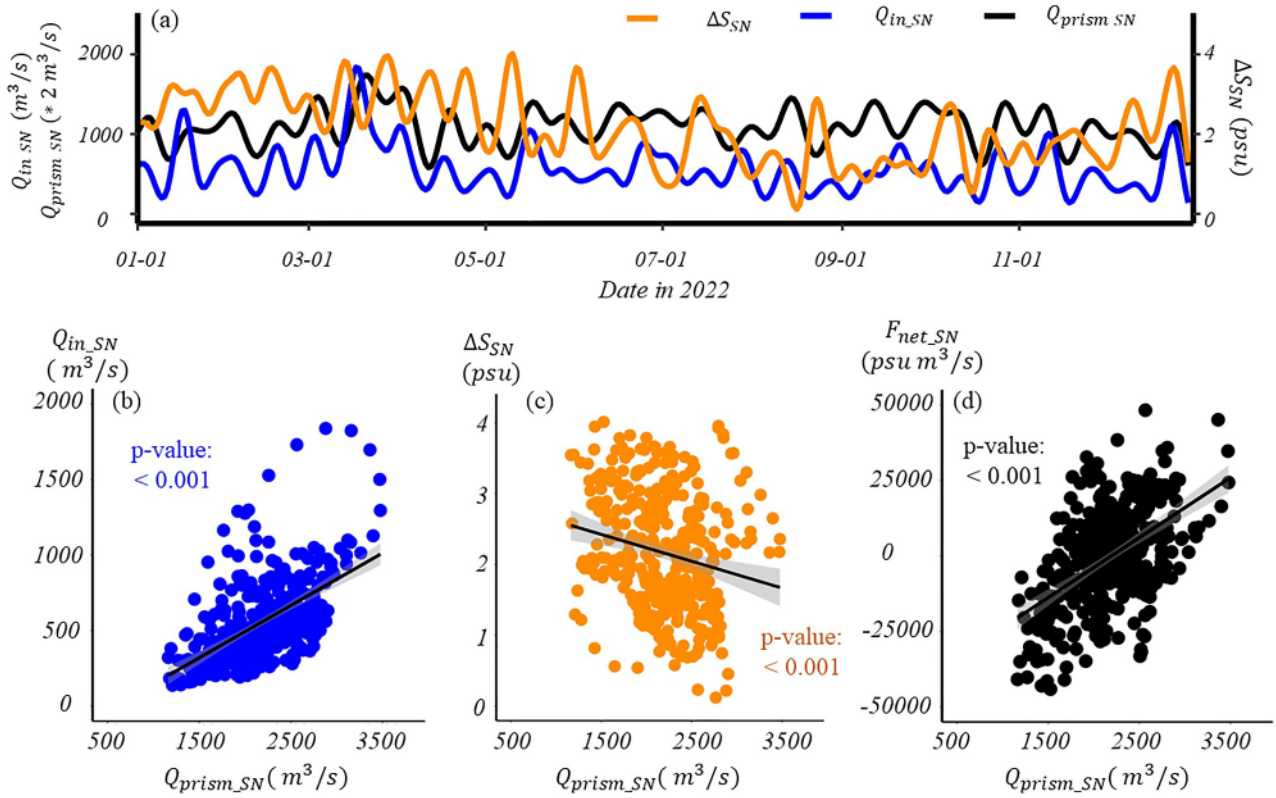

Figure 11. *Top*: time series from the Ocracoke Inlet transect of (a) Q_{in_SN} (blue), ΔS_{SN} (dark orange) and, tidal prism (Q_{prism}, black). *Bottom*: tidal prism (Q_{prism_SN}) versus (a) Q_{in_SN}, (b) ΔS_{SN}, and (c) F_{net} at the Ocracoke Inlet transect. The linear regression lines and the p-values are also shown. These values are calculated from the results for the year 2022 from the "Standard" model (Table 4). The location of Ocracoke Inlet (transect 3 in Figure 1b) and the defined direction of inward volume transport are shown in Figure 1b.

increasing (positive slope) trends exist that align with the theoretical scaling summarized in Table 1, rather than to establish strong linear correlations (i.e., a high R^2 value).

Figure 11a presents the time series of Q_{in_SN} and ΔS_{SN} along with Q_{prism_SN}. In general, when Q_{prism_SN} increases, Q_{in_SN} also increases, while ΔS_{SN} decreases. In agreement with the scaling of current-salinity tidal correlation (Table 1), the results in Figure 11b confirm a statistically significant increasing trend between Q_{in_SN} and Q_{prism_SN} (p-value <0.001, positive slope), supporting the conclusion that the tidal currents are important in driving exchange flow. Similarly, in Figure 11c, the statistically significant (p-value <0.001) decreasing (negative slope) trend between ΔS_{SN} and Q_{prism_SN} aligns with the theoretical current-salinity tidal correlation scaling summarized in Table 1. Together, these results (Figures 11b and 11c) confirm the influence of tidal transport on estuarine exchange flow at Ocracoke Inlet. Additionally, the net salt flux (F_{net_SN}) increases as Q_{prism_SN} increases, indicating higher salt flux into the estuary from tidal oscillatory salt transport at stronger tide. The same analyses are conducted for the other two inlets with similar results (Figures S7 and S8 in Supporting Information S1), confirming the role of tidal currents and their correlation with salinity in controlling the estuarine exchange flow and salt transport at the inlets.

Figure 12a presents $Q_{in\_residual}$ (blue) along with $\frac{\partial \eta}{\partial t}$ (black). $Q_{in\_residual}$ follows the trend of $\frac{\partial \eta}{\partial t}$ but with varying time lags. For instance, the time lag between the variation in $\frac{\partial \eta}{\partial t}$ and the corresponding change in $Q_{in\_residual}$ is minimal from mid-March to mid-April, whereas it increases to several days from mid-September to mid-November. This variation suggests changes in estuarine adjustment time in response to external forcings, similar to those observed in previous studies (Hetland & Geyer, 2004; MacCready, 1999, 2004, 2007). Despite the variability in time lag, Figure 12b identifies a statistically significant (p-values <0.001) increasing (positive slope) trend between the estuarine exchange flow ($Q_{in\_residual}$) and $\frac{\partial \eta}{\partial t}$, highlighting the additional influence of subtidal water level on the water exchange between the APES and the coastal ocean at the inlets. Additionally, as

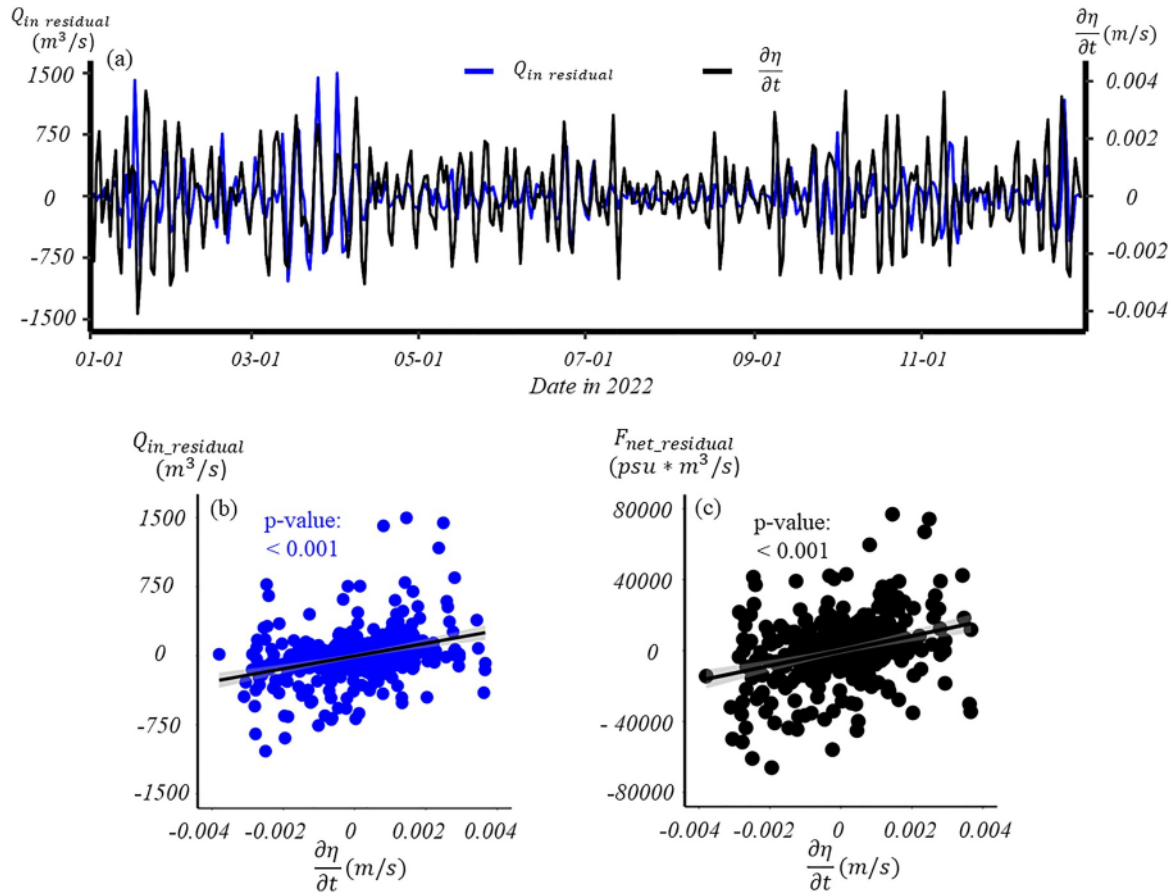

Figure 12. (a) Time series from the Ocracoke Inlet transect of $Q_{in\_residual}$ (blue) along with $\frac{\partial \eta}{\partial t}$ (black). (b) $\frac{\partial \eta}{\partial t}$ versus $Q_{in\_residual}$, and (c) $\frac{\partial \eta}{\partial t}$ versus $F_{net\_residual}$. The linear regression lines and the p-values are also shown. These values are calculated from the results of the year 2022 from the "Standard" model (Table 4). The location of Ocracoke Inlet (transect 3) and the defined direction of inward volume transport are shown in Figure 1b.

shown in Figure 12c, the residual component of the net salt flux ($F_{net\_residual}$) exhibits a significant (p-values <0.001) increasing (positive slope) trend with $\frac{\partial \eta}{\partial t}$, indicating that subtidal water level variations contribute to salt transport through the inlets alongside tidal oscillatory salt flux. The analyses are conducted for the other two inlets with similar results (Figures S9 and S10 in Supporting Information S1).

4.1.3. Albemarle Sound: The Role of Residual Water Level Variation ($\frac{\partial \eta}{\partial t}$)

Figure 13a compares the subtidal inward (Q_{in}, blue) and outward (Q_{out}, gray) volume transport against $\frac{\partial \eta}{\partial t}$ at the Albemarle Sound transect. In general, the temporal variations of Q_{in} (blue) and Q_{out} (gray) follow the trend of $\frac{\partial \eta}{\partial t}$ (orange). Additionally, the subtidal volume transport is mainly inward (i.e., comes into the estuary) and Q_{in} increases with $\frac{\partial \eta}{\partial t}$ when the latter is positive, while the subtidal volume transport is mainly outward (i.e., leaves the estuary) and Q_{out} increases when $\frac{\partial \eta}{\partial t}$ is negative. The property-property plots (Figures 13b and 13c) show that the exchange flow and net salt flux follow the scaling with $\frac{\partial \eta}{\partial t}$ (Table 1). This indicates that the barotropic salt flux, resulting from the advection of salinity filed by the barotropic flow, controls the exchange flow and net salt flux in and out of Albemarle Sound.

4.1.4. Salt Content Response

To understand the salt content response, we conduct wavelet analysis on the salt content time series shown in Figure 4. The averaged wavelet power spectra of the salt content time series (Figure 14a) shows that only the salt content in Albemarle Sound (blue) exhibits significant variations at the short unsteady timescale, with two peaks

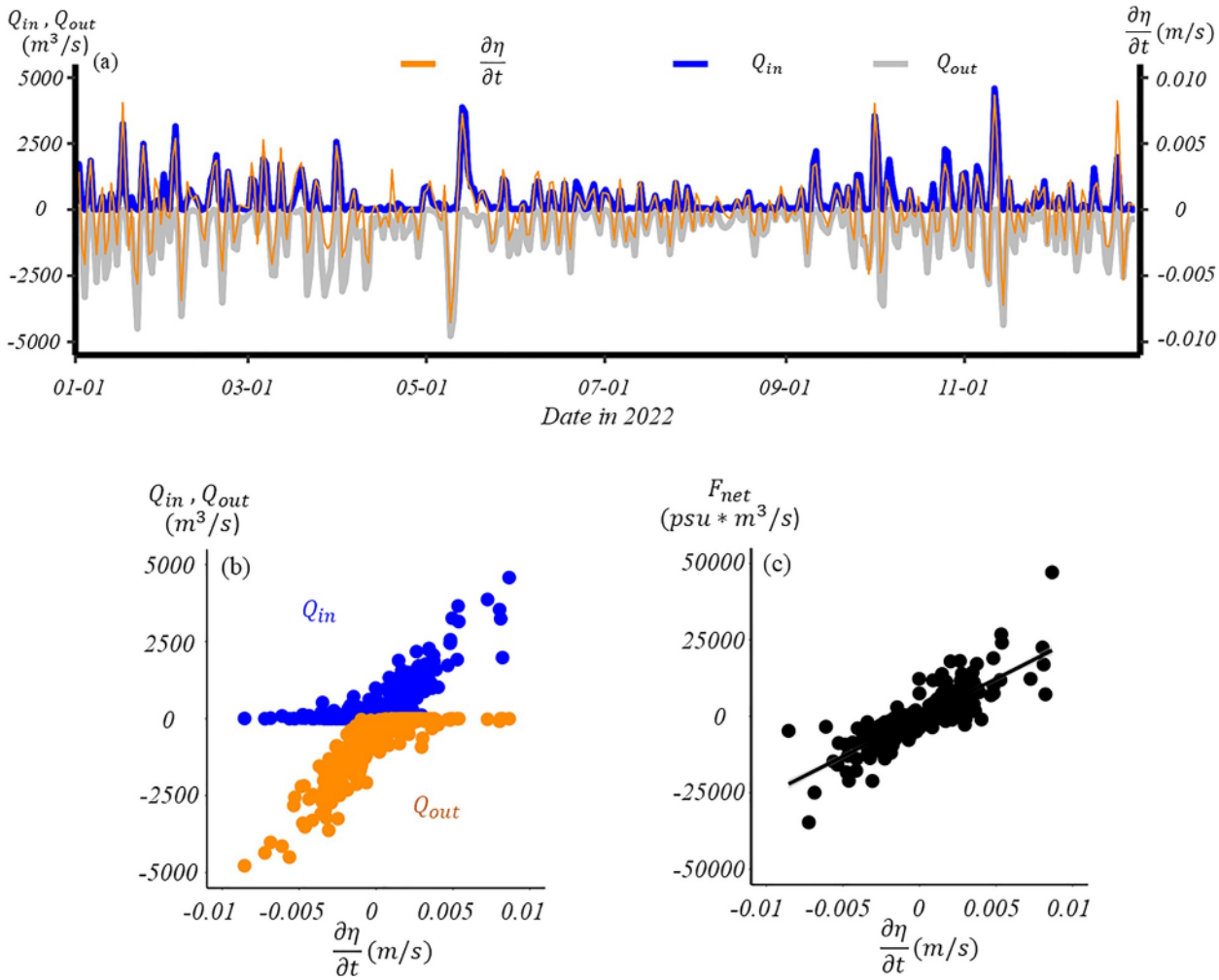

Figure 13. (a) Time series of Q_{in} (blue) and Q_{out} (gray) along with $\frac{\partial \eta}{\partial t}$ (orange) at the Albemarle Sound transect during 2022. (b) Q_{in} (blue) and Q_{out} (orange) versus $\frac{\partial \eta}{\partial t}$. (c) F_{net} versus $\frac{\partial \eta}{\partial t}$. In (c), the linear regression line and the p-value are shown. These values are calculated from the results for the year 2022 from the "Standard" model (Table 4). The location of the Albemarle Sound transect (transect 7 in Figure 1b), and the defined direction of inward volume transport are shown in Figure 1b.

of wavelet power identified at periods of ~6 and ~16 days. However, the APES (black), Pamlico River estuary (red), and Neuse River estuary (orange) exhibit minimal variations in salt content at such timescale. This indicates their differences in the response to variation of estuarine exchange flow at the short unsteady timescale, which are associated with the estuarine adjustment time.

The estuarine adjustment time for the entire APES and its sub estuaries are calculated using Equation 8 and shown in Figure 14b. Albemarle Sound has a mean estuarine adjustment time of 4 days (0.1–14 days), which is comparable to the timescale at which the estuarine exchange flow and the dominant forcing ($\frac{\partial \eta}{\partial t}$) varies. However, the mean estuarine adjustment time of the APES, the Pamlico River estuary, and the Neuse River estuary are 120 days (3–627 days), 119 days (3–460 days), and 126 days (3–496 days), respectively, which greatly exceed the short unsteady timescale. This explains why the salt content in Albemarle Sound is more responsive to changes in estuarine exchange flow at a timescale shorter than the spring-neap cycle, while the APES and the two tributary estuaries are less sensitive.

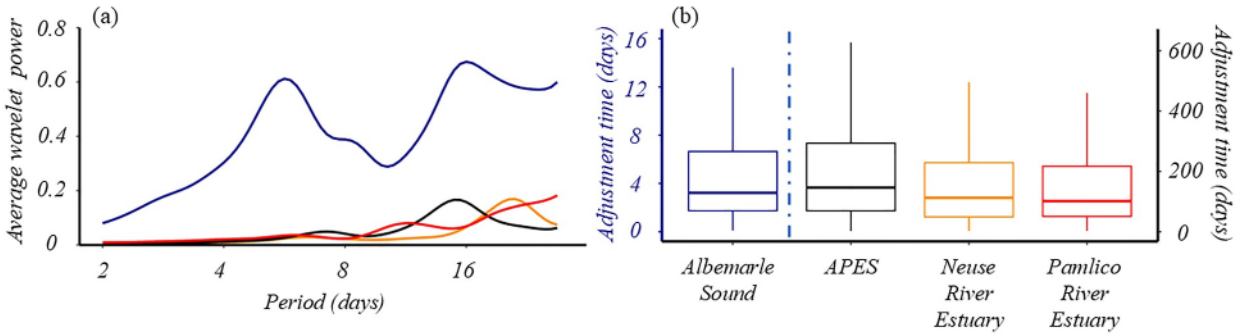

Figure 14. (a) Averaged wavelet power of the Albemarle-Pamlico estuarine system (APES) (black), Pamlico River estuary (red), Neuse River estuary (orange), and Albemarle Sound (blue). (b) The boxplots show the estuarine adjustment time of the APES (black), Pamlico River estuary (red), Neuse River estuary (orange), and Albemarle Sound (blue). Note that the left *y*-axis in (b) is for Albemarle Sound while the right *y*-axis is for the APES and the two tributary estuaries. These values are calculated from the results for the year 2022 from the "Standard" model (Table 4).

4.2. Quasi-Steady Timescale: Controlling Mechanisms and Salt Content Response

4.2.1. Sensitivity to River Discharge and Controlling Mechanisms

In this section, we discuss the control of river discharge on estuarine exchange flow and associated volume and salt transport at quasi-steady state using annual averages based on the results of sensitivity tests to discharge level (Table 4).

Figure 15 compares the annual-averaged values of Q_{in} (Figure 15a), ΔS (Figure 15b), and $Q_{in} * \Delta S$ (Figure 15c) against the normalized river discharge based on results from numerical experiments that varied river discharge over a wide range (Table 4). At the three inlets and two tributary estuaries (the Neuse River and Pamlico River estuaries), both Q_{in} and ΔS increase with the increased river discharge, which is similar to reports from previous studies of the Chesapeake Bay (Xiong et al., 2021) and Mobile Bay (Du et al., 2018). However, at Albemarle Sound, increases in river discharge lead to decreases in both Q_{in} and ΔS. This is due to the dominance of barotropic flow in controlling the water exchange between Albemarle Sound and its connecting waters. The increase in river discharge can suppress the baroclinic gradient-induced flow and reduce stratification, resulting in the decrease in Q_{in} and ΔS. Likewise, the exchange flow-induced salt flux ($Q_{in} * \Delta S$) increases with river discharge at all transects except the Albemarle Sound transect.

Additionally, the scaling relationships in Figure 15 indicate the physical mechanisms through which river discharge affects exchange flow and associated salinity differences. At the Pamlico River estuary and the Neuse River estuary, the annual averages of Q_{in} (Figure 15a) and ΔS (Figure 15b) scale with river discharge following a power-law relationship. This indicates that for the Neuse and Pamlico River estuaries, water column straining and enhanced gravitational circulation are the primary mechanisms through which river discharge impacts estuarine exchange flow, salinity difference, and the associated salt transport at long quasi-steady timescales (Table 2). However, at the three inlets and Albemarle Sound, Q_{in} (Figure 15a) and ΔS (Figure 15b) scale linearly with river discharge. This implies that the impact of river discharge on water exchange and salt transport between the APES and the open ocean through the inlets, and between Albemarle Sound and the connecting waters are mainly through its influence on barotropic flow (Table 2).

4.2.2. Salt Content Response

Figure 16a shows that the annual-averaged salt content of the APES, and its sub-basins decrease in response to increased river discharge for the sensitivity tests (Table 4). This is true even in the APES, and Pamlico and Neuse River estuaries, where increased river discharge enhances exchange flows and associated salt flux (Figure 15c, $Q_{in} * \Delta S$). The freshwater increase from the rivers more than compensate for the increased exchange flow, leading to a net decrease in salinity. Under quasi-steady state conditions, the salt balance equation can be written as Equation 5, where $Q_{in}\,\Delta S$ brings salt water into the estuary while $Q_R S_{out}$ removes salt water. Although $Q_{in}\,\Delta S$ (Figure 15c) and $Q_R S_{out}$ (Figure 16b) both increase with the increase in river discharge, the latter dominated over the former causing a net decrease in salt content (Figure 16c). For Albemarle Sound, $Q_{in}\,\Delta S$ decreases with

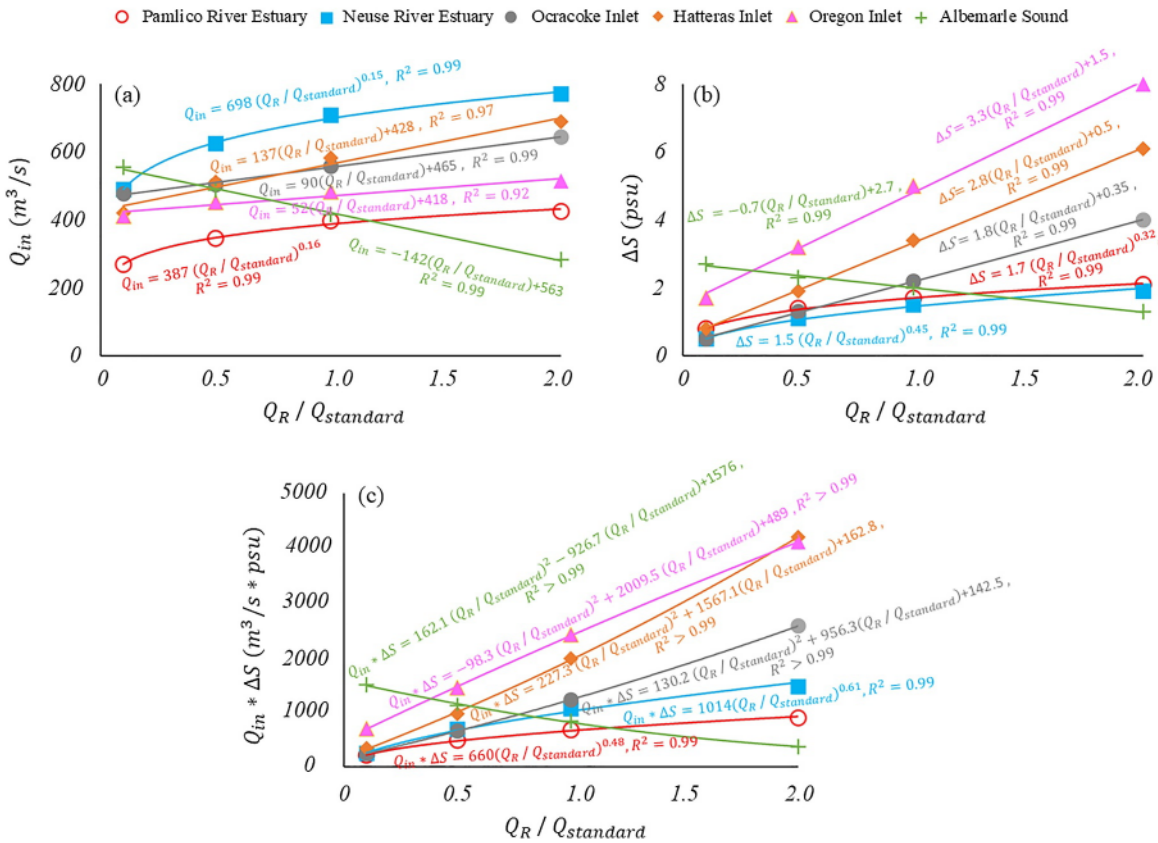

Figure 15. (a) Annual-averaged Q_{in} calculated at transects over different part of the Albemarle-Pamlico estuarine system based on the numerical model results of the year 2022 from the "Standard" and "River 1–3" experiments (Table 4). $Q_{standard}$ represents the realistic river forcing, and Q_R represents the realistic or modulated river forcings used in the numerical experiments. The equations of the best fitting lines and the correlation coefficients are also shown. (b) Same as (a) but for ΔS. (c) Same as (a) but for $Q_{in} * \Delta S$. The locations of the transects are shown in Figure 1b.

increased river discharge (Figure 15c) while $Q_R S_{out}$ is at its highest for the "Standard" run and is lower for the sensitivity tests that increased or decreased river discharge (Figure 16b). The dramatic decrease in $Q_R S_{out}$ (Figure 16b) with doubled river discharge ("River 3" in Table 4) compared to the "Standard" model (Table 4) is due to the large decrease in S_{out}. The doubled river discharge overwhelmed the annual mean estuarine circulation that pulls salt water into the estuary; meanwhile, the sound became fresher (Figure 16a), leaving less salt to lose from barotropic flow.

4.3. Implications for Biogeochemistry: Flushing Efficiency and Material Exchange

The flushing of an estuary refers to the renewal of estuarine water through river input and exchange flow. The estuarine flushing efficiency thus represents the rate of the estuary in renewing its waters, which is often quantified using the concept of flushing time (T_f). The flushing time can be defined as the average amount of time the materials such as nutrients, pollutants, and oxygen will reside in an estuary before leaving (Lucas & Delersnijder, 2020). A simple method to estimate the estuarine flushing time uses a box model approach, where T_f is estimated as $T_f = \frac{V}{Q}$, where Q is the net flux into the estuary. If the flushing is only driven by the river discharge, T_f would equal the time needed for the river discharge to fill the estuary, that is, $T_f = \frac{V}{Q_R}$. However, if we consider estuarine exchange flow and assume that Q_{in} represents the rate new ocean water entering the estuary, T_f would be $\frac{V}{Q_{in}+Q_R}$. The ratio of the flushing time under these two conditions is $\frac{Q_{in}+Q_R}{Q_R} = \alpha_R + 1$. Here, α_R is defined as the river amplification factor as presented in Section 3.4, and it thus indicates the effect of estuarine exchange flow in reducing the flushing time of the estuary, that is, enhancing the estuarine flushing efficiency. In this section, we use our model results for the year 2022 to estimate the annual mean flushing time of the APES and

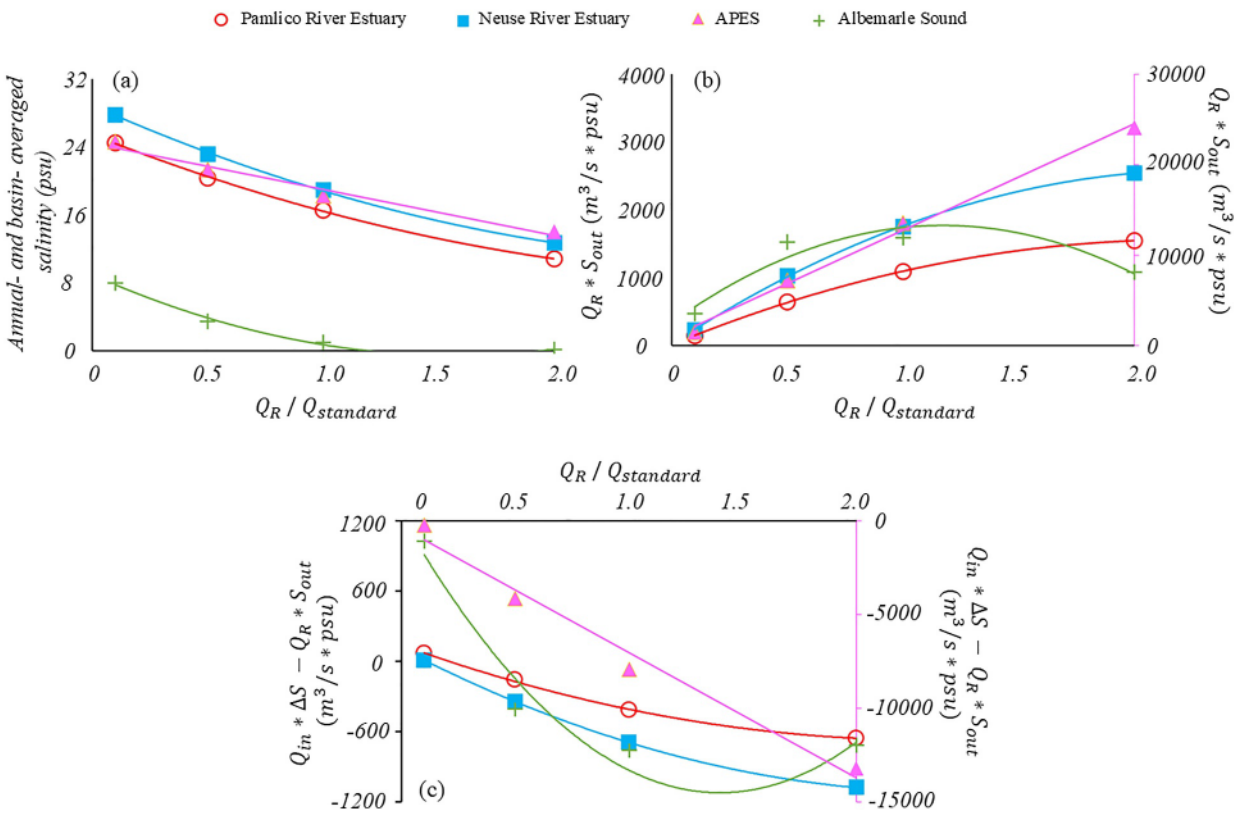

Figure 16. (a) Annual-averaged salt content of the Albemarle-Pamlico estuarine system (APES) and its sub-basins based on results of the numerical model for 2022 from the "Standard" and "River 1–3" models (Table 4). $Q_{standard}$ represents the realistic river forcing for 2022 used in the "Standard" model, whereas Q_R was the river discharge used for sensitivity experiments (Table 4). (b) Same as (a) but for the salt flux associated with river discharge ($Q_R * S_{out}$). (c) Same as (a) but for the net salt flux (i.e., $Q_{in} * \Delta S - Q_R * S_{out}$). Note that (b) and (c) used two *y*-axes; the *y*-axis on the right is for the APES.

its sub-basins, and investigate the amplification effect of estuarine exchange flow on the flushing time and its response to varying river discharge.

As shown in Figure 17a, based on results of the year 2022 from the "Standard" model, the annual mean flushing time of the APES, Albemarle Sound, Neuse River estuary, and Pamlico River estuary are 190 days, 120 days, 22 days, and 29 days, respectively, which agree with previous reported values (Stanley, 1992; Wells & Kim, 1989). The river amplification factors α_R are 3.6, 9.1, and 7.6 for the APES, Neuse River estuary, and Pamlico River estuary, respectively. This indicates that the estuarine exchange flow has significantly reduced the flushing time of the APES and its two tributary estuaries (i.e., Pamlico and Neuse). The α_R for Albemarle Sound is only 1.3, however, indicating the less significant role of estuarine exchange flow in flushing this estuary.

Additionally, with the increased river discharge, the flushing time of the APES and its sub-basins decreased. For the APES and its two tributary estuaries (i.e., Pamlico and Neuse), T_f follows a power-law relationship with Q_R (Figure 17a), in a manner similar to reports from a previous study of Mobile Bay (Du et al., 2018). The power-law relationship between T_f and Q_R indicates the control of estuarine exchange flow (Q_{in}), which also follows a power-law relationship with Q_R (Figure 17b), on the estuary flushing time in the APES and its two tributary estuaries. However, for Albemarle Sound, T_f follows a linear relationship with Q_R (Figure 17a) while the exchange flow (Q_{in}) follows a power-law relationship with Q_R (Figure 17b), which is due to the dominant role played by the river discharge in the flushing of Albemarle Sound, as also evidenced by the small river amplification factor discussed above.

Neuse and Pamlico River estuaries have the shortest flushing times (Figure 17a, blue and red lines) and the largest amplification ratios (Figure 17b, blue and red lines). This suggests that their biogeochemical processes can be significantly affected by the estuarine exchange flow, a factor that has been overlooked in previous studies. And the effect the estuarine exchange flow in regulating biogeochemistry in Neuse and Pamlico River estuaries is

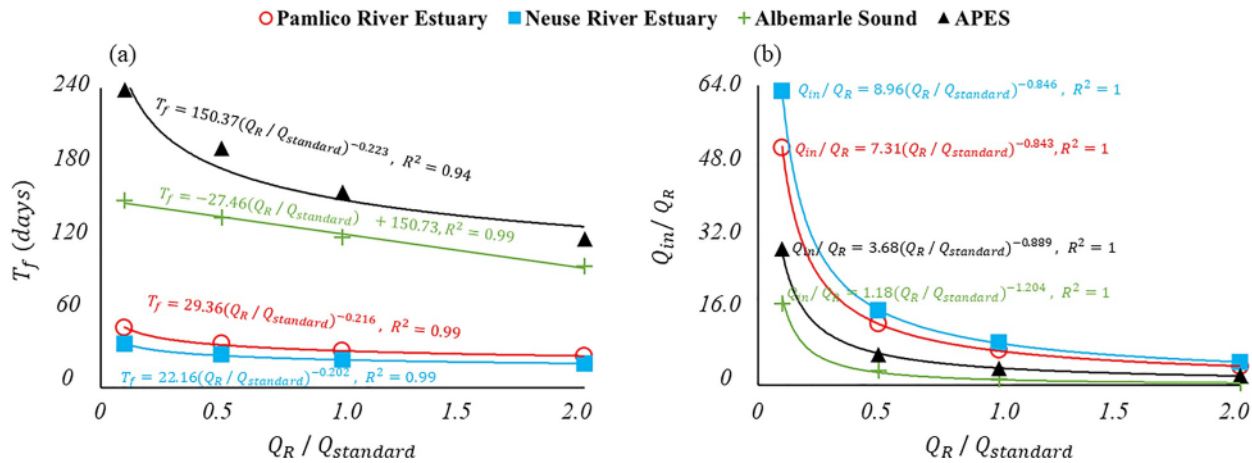

Figure 17. (a) Annual mean flushing time of the Albemarle-Pamlico estuarine system, the Albemarle Sound, and the two tributary estuaries calculated based on the numerical model results of the year 2022 from the "Standard" and "River 1–3" experiments (Table 4). $Q_{standard}$ represents the realistic river forcing, and Q_R represents the realistic or modulated river forcings used in the numerical experiments. (b) Same as (a) but for α_R (Q_{in}/Q_R).

likely to remain important during both dry and normal years, as their amplification ratios remain high. In contrast, Albemarle Sound has longer flushing time (Figure 17a, green line) and the lowest amplification ratio (Figure 17b, green line). This indicates that in terms of estuary flushing, river discharge plays a primary role in Albemarle Sound. This condition is expected to remain unless the river discharge becomes substantially low (e.g., $\frac{Q_R}{Q_{standard}} < 0.5$), which is unlikely given that the year 2022 is already one of the driest years in the past two decades (Figure S1 in Supporting Information S1).

The variation in flushing time across the APES and its sub-basins indicates a potential spatial gradient in geochemical processing within the system. For example, flushing time increases substantially along the continuum between the tributary estuaries and the Pamlico Sound sub-basin. As a result, a significant portion of land-derived nutrients and organic carbon maybe transported to Pamlico Sound before undergoing substantial decomposition in the tributary estuaries. This effect is likely amplified during periods of high river discharge, which increase material loading while reducing flushing time in the upper estuaries (Figure 17). Given its longer flushing time, Pamlico Sound may function as a biogeochemical reactor of terrestrial inputs, acting as a hotspot for carbon transformation and primary productivity fueled by nutrient delivery from the Neuse and Pamlico Rivers. Compared to the Neuse and Pamlico River estuaries, the much longer flushing time of Albemarle Sound likely allows for more extensive in situ decomposition of organic matter originating from the Chowan and Roanoke Rivers before it reaches Pamlico Sound or is exported through Oregon Inlet to the coastal ocean.

In addition to affecting flushing efficiency, estuarine exchange flow likely plays a key role in regulating the exchange of biologically important materials between the APES and the coastal ocean, as well as among its sub-basins. For instance, fish larvae and juveniles can be transported into the APES from the coastal ocean and redistributed across its sub-basins via the estuarine exchange flow (e.g., Hettler Jr & Barker, 1993; Pietrafesa, Janowitz, Chao, et al., 1986; Pietrafesa, Janowitz, Miller, et al., 1986). Variations in the estuarine exchange flow at different timescales and under different forcing conditions as presented in this study can thus significantly affect the recruitment, retention, and export of fish larvae in the APES. As discussed in Sections 4.1.2 and 4.1.3, wind-induced residual water levels play a significant role in controlling the estuarine exchange flow both at the inlets and in Albemarle Sound. Therefore, certain wind conditions may enhance the recruitment of fish larvae from the coastal ocean into the APES through the inlets, and further into Albemarle Sound and the tributary estuaries. Seasonal changes in wind conditions may therefore lead to variations in estuarine exchange flow and fish larvae recruitment in the APES.

Moreover, the APES receives nutrient inputs from the Neuse and Pamlico Rivers, contributing to the development of hypoxia and harmful algal blooms (Buzzelli et al., 2002; Paerl, 1997). Previous studies have reported correlations between hypoxia development and river discharge, as well as wind stress (e.g., Paerl et al., 2010; Paerl et al., 2014; Stanley & Nixon, 1992). Winds are commonly recognized as a factor that disrupts water column

stratification and increases bottom oxygen concentration (e.g., Stanley & Nixon, 1992). However, our study suggests that down-estuary winds (below a certain intensity) may contribute to the salinity difference between the surface inflow and bottom outflow, thereby increasing water column stratification in both the Pamlico and Neuse River estuaries. This highlights the complex role winds may play in regulating biogeochemistry in the tributary estuaries, which may require further investigation.

5. Summary and Conclusions

In this study, we investigated the variation of estuarine exchange flow in the APES and its sub-basins at both unsteady short (meteorological band and spring-neap cycle) and longer quasi-steady (annual mean) timescales using a three-dimensional hydrodynamic model and a TEF analysis framework. The major mechanisms behind the estuarine exchange flow were interpreted using previously developed theoretical scalings (Chen et al., 2012; MacCready & Geyer, 2024; Ralston et al., 2008). Additionally, the response of salt content in the estuary to the variation of estuarine exchange flow at these unsteady and quasi-steady timescales were also discussed. Moreover, we discussed the implications of the estuarine exchange to biogeochemistry in the APES. This was the first time such an analysis has been done for this estuary. Overall, the model results showed the following:

1. *For the inlets*, (a) at the short unsteady timescales ranging from subtidal to the spring/neap, estuarine exchange flow is controlled by the combination of current-salinity tidal correlation and the time rate of change in residual water level ($\frac{\partial \eta}{\partial t}$ in Table 1). The magnitudes of estuarine exchange flow and net salt transport from the two mechanisms are comparable. The volume transport and net salt transport due to tidal oscillatory motion increase with stronger tides, following the scaling of current-salinity tidal correlation (Table 1). The volume and net salt transport associated with the residual water level increases as the time rate of the change of residual water level increases, following the scaling with $\frac{\partial \eta}{\partial t}$ (Table 1). The salt content of the whole APES system exhibits little response to the variation in estuarine exchange flow at these unsteady short timescales because of its much longer estuarine adjustment time (~hundreds of days). (b) At long quasi-steady timescales based on the annual averages, river discharge controls the estuarine exchange flow at the inlets via barotropic flow. Increased river discharge increases the volume transport, salinity difference, and salt transport due to estuarine exchange flow. The salt content of the whole APES system decreases with increased river discharge because the salt loss from barotropic flow exceeds the salt gain from estuarine exchange flow.
2. *The Neuse River and Pamlico River estuaries* exhibit similar dynamics. (a) At the unsteady timescale (meteorological band), the estuarine exchange flow is controlled by wind-induced straining. Increased down-estuary wind enhances the volume transport, salinity difference between the inward and outward volume transport, as well as the salt transport associated with the estuarine exchange flow, following the scaling of wind straining (Table 1). However, the net salt transport tends to decrease with increased down-estuary wind, due to the salt loss from the decreased volume of the estuary. Their salt contents are not responsive to the variations in estuarine exchange flow at the short unsteady timescale due to their longer estuarine adjustment times (~hundreds of days). (b) At long quasi-steady timescales, river discharge controls the estuarine exchange flow through gravitational circulation. Increased river discharge increases the volume transport, salinity difference, and salt transport due to estuarine exchange flow. Salt contents of the two estuaries decreases with increased river discharge because the salt loss from barotropic flow greatly exceeds the salt gained from estuarine exchange flow.
3. *Albemarle Sound* behaves differently than the Neuse River and Pamlico River estuaries. For Albemarle Sound, (a) at the short unsteady timescales (subtidal through spring/neap), the estuarine exchange flow is controlled by the time rate of change of residual water level. The salt transport of the estuarine exchange flow differs during times of rising versus falling water levels. Salt transport is minimal when residual water level at the estuary mouth is decreasing. However, when the residual water level at the estuary's mouth is increasing, the salt transport of the estuarine exchange flow is oceanward and increases with the time rate of change in residual water level. The estuarine adjustment time of ~ a few days is comparable to the meteorological band, resulting in significant variation in salt content at these timescales. (b) At long quasi-steady timescales, river discharge controls Albemarle Sound's estuarine exchange flow through barotropic flow. Increased river discharge decreases the volume transport, salinity difference, and salt transport via estuarine exchange flow. Salt content

decreases with increased river discharge because of increased salt loss from barotropic flow and decreased salt input due to estuarine exchange flow.

4. At annual timescale, the estuarine exchange flow likely plays a dominant role in flushing of APES and its two tributary estuaries, while in Albemarle Sound, the river discharge regulates the flushing.

Our results highlight the spatial heterogeneity of the controlling mechanisms behind estuarine exchange flow and their dependence on timescales in the APES. Due to its complex geometry, defining the estuarine length of the APES is challenging, making it difficult to apply existing exchange flow scaling frameworks that classify estuaries as either long or short (Chen et al., 2012). Additionally, different subdomains of the APES respond variably to dominant forcing mechanisms, complicating efforts to categorize the entire system under a single exchange flow regime, whether driven by gravitational circulation or tidal currents (MacCready & Geyer, 2024). Furthermore, we found that the estuarine adjustment time of salt content varies significantly across different regions of this large lagoonal estuary, ranging from days to annual timescales. Understanding salt content dynamics in a lagoonal estuary like the APES thus requires careful consideration of spatial variations in estuarine adjustment times, dominant forcing timescales, and their relative magnitudes. The APES provides an example of a large lagoonal estuary having relatively shallow depths, micro- to meso-tides, and multiple inlets and subbasins. Understanding its exchange dynamics will be useful for future research on similar systems.

Our results also indicate the potentially important yet overlooked role that estuarine exchange flow plays in influencing the biogeochemistry of the APES and its two tributary estuaries (Pamlico and Neuse) through its regulation of flushing efficiency and material exchange. We therefore emphasize that future efforts are needed to better quantify the impact of estuarine exchange flow on the biogeochemical processes in the APES. The results from such efforts will help evaluate the relative importance of different inputs (i.e., river VS exchange flow) in contributing to the development of environmental issues that often occur in the APES, and lead to better management of the system.

Acknowledgments

Research ideas for this study were inspired by the poster presentation that Dr. Parker MacCready (University of Washington) gave in 2023 Gordon Research Conference. The authors thank Dr. David Ralston (Woods Hole Oceanographic Institution), Dr. Neil Ganju (United States Geological Survey), Dr. Jilian Xiong (University of Washington), and Dr. Rocky Geyer (Woods Hole Oceanographic Institution) for many insightful discussions related to this work. Dr. Christie Hegermiller (University of Washington) is thanked for helping with the model setup. We would like to thank North Carolina Department of Environmental Quality (Dr. David Huffman and Dr. Susan Gale) and the Paerl Lab at the University of North Carolina-Chapel Hill (Dr. Hans Paerl, Dr. Karen Rossignol, and Dr. Randy Sloup) for providing the salinity observation data. Dr. Stephen Moysey and Dr. Mike O'Driscoll (both from East Carolina University) are thanked for many useful discussions on the Albemarle-Pamlico Estuarine System. This material is based upon work supported by the National Science Foundation under Grant 2052889. Any opinions, findings, and conclusions or recommendations expressed in this material are those of the author(s) and do not necessarily reflect the views of the National Science Foundation. The authors acknowledge William & Mary Research Computing for providing computational resources and technical support that have contributed to the results reported within this paper.

Data Availability Statement

The salinity data from the Modeling and Monitoring Project can be accessed via the SECOORA Data Portal (https://portal.secoora.org/?#metadata/190/sensor_source/inventory). Hourly river discharge can be accessed through the USGS National Water Information System (https://waterdata.usgs.gov/nwis). Model data sets are publicly available through the William & Mary Scholar Works (https://www.doi.org/10.25773/h1q6-pr14, Yin et al., 2025).

References

Banas, N. S., Hickey, B. M., MacCready, P., & Newton, J. A. (2004). Dynamics of Willapa Bay, Washington: A highly unsteady, partially mixed Estuary. *Journal of Physical Oceanography*, *34*(11), 2413–2427. https://doi.org/10.1175/JPO2637.1

Barlow, J. P. (1956). Effect of wind on salinity distribution in an estuary. *Journal of Marine Research*, *15*(3), 193–203. https://elischolar.library.yale.edu/journal_of_marine_research/873/

Bowen, M. M., & Geyer, W. R. (2003). Salt transport and the time-dependent salt balance of a partially stratified estuary. *Journal of Geophysical Research*, *108*(C5), 3158. https://doi.org/10.1029/2001JC001231

Burchard, H., & Hetland, R. D. (2010). Quantifying the contributions of tidal straining and gravitational circulation to residual circulation in periodically stratified tidal estuaries. *Journal of Physical Oceanography*, *40*(6), 1243–1262. https://doi.org/10.1175/2010JPO4270.1

Buzzelli, C. P., Luettich Jr, R. A., Powers, S. P., Peterson, C. H., McNinch, J. E., Pinckney, J. L., & Paerl, H. W. (2002). Estimating the spatial extent of bottom-water hypoxia and habitat degradation in a shallow estuary. *Marine Ecology Progress Series*, *230*, 103–112. https://doi.org/10.3354/meps230103

Chatwin, P. C. (1976). Some remarks on the maintenance of the salinity distribution in estuaries. *Estuarine and Coastal Marine Science*, *4*(5), 555–566. https://doi.org/10.1016/0302-3524(76)90030-X

Chen, S. N., Geyer, W. R., Ralston, D. K., & Lerczak, J. A. (2012). Estuarine exchange flow quantified with isohaline coordinates: Contrasting long and short estuaries. *Journal of Physical Oceanography*, *42*(5), 748–763. https://doi.org/10.1175/JPO-D-11-086.1

Chen, S. N., & Sanford, L. P. (2009). Axial wind effects on stratification and longitudinal salt transport in an idealized, partially mixed estuary. *Journal of Physical Oceanography*, *39*(8), 1905–1920. https://doi.org/10.1175/2009JPO4016.1

Clunies, G. J., Mulligan, R. P., Mallinson, D. J., & Walsh, J. P. (2017). Modeling hydrodynamics of large Lagoons: Insights from the Albemarle-Pamlico Estuarine System. *Estuarine, Coastal and Shelf Science*, *189*, 90–103. https://doi.org/10.1016/j.ecss.2017.03.012

Conroy, T., Sutherland, D. A., & Ralston, D. K. (2020). Estuarine exchange flow variability in a seasonal, segmented estuary. *Journal of Physical Oceanography*, *50*(3), 595–613. https://doi.org/10.1175/JPO-D-19-0108.1

Cook, S. E., Warner, J. C., & Russell, K. L. (2023). A numerical investigation of the mechanisms controlling salt intrusion in the Delaware Bay estuary. *Estuarine, Coastal and Shelf Science*, *283*, 108257. https://doi.org/10.1016/j.ecss.2023.108257

Du, J., Park, K., Shen, J., Dzwonkowski, B., Yu, X., & Yoon, B. I. (2018). Role of baroclinic processes on flushing characteristics in a highly stratified estuarine system, Mobile Bay, Alabama. *Journal of Geophysical Research: Oceans*, *123*(7), 4518–4537. https://doi.org/10.1029/2018JC013855

Epperly, S. P., & Ross, S. W. (1986). *Characterization of the North Carolina Pamlico-Albemarle estuarine complex* (Vol. 175). US Department of Commerce, National Oceanic and Atmospheric Administration, National Marine Fisheries Service, Southeast Fisheries Center. Beaufort Laboratory.

Fagherazzi, S., Anisfeld, S. C., Blum, L. K., Long, E. V., Feagin, R. A., Fernandes, A., et al. (2019). Sea level rise and the dynamics of the marsh-upland boundary. *Frontiers in Environmental Science*, *7*, 25. https://doi.org/10.3389/fenvs.2019.00025

Feng, Z., & Li, C. (2010). Cold-front-induced flushing of the Louisiana Bays. *Journal of Marine Systems*, *82*(4), 252–264. https://doi.org/10.1016/j.jmarsys.2010.05.015

Fischer, H. B., List, J. E., Koh, C. R., Imberger, J., & Brooks, N. H. (1979). *Mixing in inland and coastal waters*. Academic Press. https://doi.org/10.1016/C2009-0-22051-4

Garvine, R. W. (1985). A simple model of estuarine subtidal fluctuations forced by local and remote wind stress. *Journal of Geophysical Research*, *90*(C6), 11945–11948. https://doi.org/10.1029/JC090iC06p11945

Getz, E., & Eckert, C. (2023). Effects of salinity on species richness and community composition in a hypersaline estuary. *Estuaries and Coasts*, *46*(8), 2175–2189. https://doi.org/10.1007/s12237-022-01117-2

Geyer, W. R. (1997). Influence of wind on dynamics and flushing of shallow estuaries. *Estuarine, Coastal and Shelf Science*, *44*(6), 713–722. https://doi.org/10.1006/ecss.1996.0140

Geyer, W. R., Ralston, D. K., & Chen, J. L. (2020). Mechanisms of exchange flow in an estuary with a narrow, deep channel and wide, shallow shoals. *Journal of Geophysical Research: Oceans*, *125*(12), e2020JC016092. https://doi.org/10.1029/2020JC016092

Geyer, W. R., & Signell, R. P. (1992). A reassessment of the role of tidal dispersion in estuaries and bays. *Estuaries*, *15*(2), 97–108. https://doi.org/10.2307/1352684

Giese, G. L., Wilder, H. B., & Parker, G. G. (1985). *Hydrology of major estuaries and sounds of North Carolina* (Vol. 2221). US Government Printing Office.

Gong, W., Shen, J., Cho, K. H., & Wang, H. V. (2009). A numerical model study of barotropic subtidal water exchange between estuary and subestuaries (tributaries) in the Chesapeake Bay during northeaster events. *Ocean Modelling*, *26*(3–4), 170–189. https://doi.org/10.1016/j.ocemod.2008.09.005

Haidvogel, D. B., Arango, H., Budgell, W. P., Cornuelle, B. D., Curchitser, E., Di Lorenzo, E., et al. (2008). Ocean forecasting in terrain-following coordinates: Formulation and skill assessment of the regional ocean modeling system. *Journal of Computational Physics*, *227*(7), 3595–3624. https://doi.org/10.1016/j.jcp.2007.06.016

Haidvogel, D. B., Arango, H. G., Hedstrom, K., Beckmann, A., Malanotte-Rizzoli, P., & Shchepetkin, A. F. (2000). Model evaluation experiments in the north Atlantic basin: Simulations in nonlinear terrain-following coordinates. *Dynamics of Atmospheres and Oceans*, *32*(3–4), 239–281. https://doi.org/10.1016/S0377-0265(00)00049-X

Hansen, D. V., & Rattray, M., Jr. (1965). Gravitational circulation in straits and estuaries. *Journal of Marine Research*, *23*, 104–122.

Hetland, R. D., & Geyer, W. R. (2004). An idealized study of the structure of long, partially mixed estuaries. *Journal of Physical Oceanography*, *34*(12), 2677–2691. https://doi.org/10.1175/JPO2646.1

Hettler Jr, W. F., & Barker, D. L. (1993). Distribution and abundance of larval fishes at two North Carolina inlets. *Estuarine, Coastal and Shelf Science*, *37*(2), 161–179. https://doi.org/10.1006/ecss.1993.1049

Huang, W., & Li, C. (2017). Cold front driven flows through multiple inlets of Lake Pontchartrain Estuary. *Journal of Geophysical Research: Oceans*, *122*(11), 8627–8645. https://doi.org/10.1002/2017JC012977

Jay, D. A., & Smith, J. D. (1990a). Residual circulation in shallow estuaries: 1. Highly stratified, narrow estuaries. *Journal of Geophysical Research*, *95*(C1), 711–731. https://doi.org/10.1029/JC095iC01p00711

Jay, D. A., & Smith, J. D. (1990b). Residual circulation in shallow estuaries: 2. Weakly stratified and partially mixed, narrow estuaries. *Journal of Geophysical Research*, *95*(C1), 733–748. https://doi.org/10.1029/JC095iC01p00733

Jia, P., & Li, M. (2012a). Circulation dynamics and salt balance in a lagoonal Estuary. *Journal of Geophysical Research*, *117*(C1). https://doi.org/10.1029/2011JC007124

Jia, P., & Li, M. (2012b). Dynamics of wind-driven circulation in a shallow lagoon with strong horizontal density gradient. *Journal of Geophysical Research*, *117*(C5). https://doi.org/10.1029/2011JC007475

Knoppers, B. (1994). Aquatic primary production in coastal Lagoons. In *Elsevier oceanography series* (Vol. 60, pp. 243–286). Elsevier. https://doi.org/10.1016/s0422-9894(08)70014-x

Kranenburg, C. (1986). A time scale for long-term salt intrusion in well-mixed estuaries. *Journal of Physical Oceanography*, *16*(7), 1329–1331. https://doi.org/10.1175/1520-0485(1986)016<1329:atsflt>2.0.co;2

Lerczak, J. A., Geyer, W. R., & Chant, R. J. (2006). Mechanisms driving the time-dependent salt flux in a partially stratified Estuary. *Journal of Physical Oceanography*, *36*(12), 2296–2311. https://doi.org/10.1175/JPO2959.1

Li, C., Huang, W., Chen, C., & Lin, H. (2018). Flow regimes and adjustment to wind-driven motions in Lake Pontchartrain Estuary: A modeling experiment using FVCOM. *Journal of Geophysical Research: Oceans*, *123*(11), 8460–8488. https://doi.org/10.1029/2018JC013985

Li, Y., & Li, M. (2011). Effects of winds on stratification and circulation in a partially mixed Estuary. *Journal of Geophysical Research*, *116*(C12), C12012. https://doi.org/10.1029/2010JC006893

Li, Y., & Li, M. (2012). Wind-driven lateral circulation in a stratified estuary and its effects on the along-channel flow. *Journal of Geophysical Research*, *117*(C9), C09005. https://doi.org/10.1029/2011JC007829

Lin, J., Xie, L., Pietrafesa, L. J., Ramus, J. S., & Paerl, H. W. (2007). Water quality gradients across albemarle-pamlico estuarine system: Seasonal variations and model applications. *Journal of Coastal Research*, *23*(1), 213–229. https://doi.org/10.2112/05-0507.1

Lucas, L. V., & Deleersnijder, E. (2020). Timescale methods for simplifying, understanding and modeling biophysical and water quality processes in coastal aquatic ecosystems: A review. *Water*, *12*(10), 2717. https://doi.org/10.3390/w12102717

Luettich Jr, R. A., Carr, S. D., Reynolds-Fleming, J. V., Fulcher, C. W., & McNinch, J. E. (2002). Semi-diurnal seiching in a shallow, micro-tidal lagoonal Estuary. *Continental Shelf Research*, *22*(11–13), 1669–1681. https://doi.org/10.1016/S0278-4343(02)00031-6

MacCready, P. (1999). Estuarine adjustment to changes in river discharge and tidal mixing. *Journal of Physical Oceanography*, *29*(4), 708–726. https://doi.org/10.1175/1520-0485(1999)029<0708:eatcir>2.0.co;2

MacCready, P. (2004). Toward a unified theory of tidally-averaged estuarine salinity structure. *Estuaries*, *27*(4), 561–570. https://doi.org/10.1007/BF02907644

MacCready, P. (2007). Estuarine adjustment. *Journal of Physical Oceanography*, *37*(8), 2133–2145. https://doi.org/10.1175/JPO3082.1

MacCready, P. (2011). Calculating estuarine exchange flow using isohaline coordinates. *Journal of Physical Oceanography*, *41*(6), 1116–1124. https://doi.org/10.1175/2011JPO4517.1

MacCready, P., & Geyer, W. R. (2010). Advances in estuarine physics. *Annual Review of Marine Science*, *2*(1), 35–58. https://doi.org/10.1146/annurev-marine-120308-081015

MacCready, P., & Geyer, W. R. (2024). Estuarine exchange flow in the Salish Sea. *Journal of Geophysical Research: Oceans*, *129*(1). https://doi.org/10.1029/2023JC020369

MacCready, P., Geyer, W. R., & Burchard, H. (2018). Estuarine exchange flow is related to mixing through the salinity variance budget. *Journal of Physical Oceanography*, *48*(6), 1375–1384. https://doi.org/10.1175/JPO-D-17-0266.1

Mesinger, F., DiMego, G., Kalnay, E., Mitchell, K., Shafran, P. C., Ebisuzaki, W., et al. (2006). North American regional reanalysis. *Bulletin of the American Meteorological Society*, *87*(3), 343–360. https://doi.org/10.1175/BAMS-87-3-343

Monismith, S. G., Kimmerer, W., Burau, J. R., & Stacey, M. T. (2002). Structure and flow-induced variability of the subtidal salinity field in northern San Francisco Bay. *Journal of Physical Oceanography*, *32*(11), 3003–3019. https://doi.org/10.1175/1520-0485(2002)032<3003:safivo>2.0.co;2

Moslow, T. F., & Heron, S. D. (1994). The outer banks of North Carolina. In R. A. Davis (Ed.), *Geology of Holocene barrier island systems* (pp. 47–74). Springer. https://doi.org/10.1007/978-3-642-78360-9_2

Mulligan, R. P., Mallinson, D. J., Clunies, G. J., Rey, A., Culver, S. J., Zaremba, N., et al. (2019). Estuarine responses to long-term changes in inlets, morphology, and sea level rise. *Journal of Geophysical Research: Oceans*, *124*(12), 9235–9257. https://doi.org/10.1029/2018JC014732

Nidzieko, N. J., & Monismith, S. G. (2013). Contrasting seasonal and fortnightly variations in the circulation of a seasonally inverse estuary, Elkhorn Slough, California. *Estuaries and Coasts*, *36*, 1–17. https://doi.org/10.1007/s12237-012-9548-1

Olson, E. M., Allen, S. E., Do, V., Dunphy, M., & Ianson, D. (2020). Assessment of nutrient supply by a tidal jet in the northern strait of Georgia based on a biogeochemical model. *Journal of Geophysical Research: Oceans*, *125*(8), e2019JC015766. https://doi.org/10.1029/2019JC015766

Paerl, H. W. (1982). *Environmental factors promoting and regulating N_2 fixing blue-green algal blooms in the chowan river, NC*. Water Resources Research Institute of the University of North Carolina.

Paerl, H. W. (1997). Coastal eutrophication and harmful algal blooms: Importance of atmospheric deposition and groundwater as "new" nitrogen and other nutrient sources. *Limnology & Oceanography*, *42*(5), 1154–1165. https://doi.org/10.4319/lo.1997.42.5_part_2.1154

Paerl, H. W., Christian, R. R., Bales, J. D., Peierls, B. L., Hall, N. S., Joyner, A. R., & Riggs, S. R. (2010). *2 Assessing the response of the Pamlico Sound, North Carolina, USA to human and climatic disturbances*. Coastal lagoons: critical habitats of environmental change, Vol. 17, 17–42. https://doi.org/10.1201/EBK1420088304-c2

Paerl, H. W., Crosswell, J. R., Van Dam, B., Hall, N. S., Rossignol, K. L., Osburn, C. L., et al. (2018). Two decades of tropical cyclone impacts on north Carolina's estuarine carbon, nutrient and phytoplankton dynamics: Implications for biogeochemical cycling and water quality in a stormier world. *Biogeochemistry*, *141*(3), 307–332. https://doi.org/10.1007/s10533-018-0438-x

Paerl, H. W., Hall, N. S., Peierls, B. L., Rossignol, K. L., & Joyner, A. R. (2014). Hydrologic variability and its control of phytoplankton community structure and function in two shallow, coastal, lagoonal ecosystems: The Neuse and new river estuaries, North Carolina, USA. *Estuaries and Coasts*, *37*(S1), 31–45. https://doi.org/10.1007/s12237-013-9686-0

Paerl, H. W., Rossignol, K. L., Guajardo, R., Hall, N. S., Joyner, A. R., Peierls, B. L., & Ramus, J. S. (2009). FerryMon: Ferry-based monitoring and assessment of human and climatically driven environmental change in the albemarle-pamlico sound system. *Environmental Science & Technology*, *43*(20), 7609–7613. https://doi.org/10.1021/es900558f

Park, K., & Kuo, A. Y. (1996). Effect of variation in vertical mixing on residual circulation in narrow, weakly nonlinear estuaries. In D. G. Aubrey & C. T. Friedrichs (Eds.), *Buoyancy effects on coastal and estuarine dynamics* (Vol. 53, pp. 301–317). American Geophysical Union. https://doi.org/10.1029/CE053p0301

Pietrafesa, L. J., Janowitz, G. S., Chao, T. Y., Weisberg, R. H., Askari, F., & Noble, E. (1986). *The physical oceanography of Pamlico Sound*. University of North Carolina Sea Grant. Retrieved from https://repository.library.noaa.gov/view/noaa/44383/noaa_44383_DS1.pdf

Pietrafesa, L. J., Janowitz, G. S., Miller, J. M., Noble, E. B., Ross, S. W., & Epperly, S. P. (1986). Abiotic factors influencing the spatial and temporal variability of juvenile fish in Pamlico Sound, North Carolina. In *Estuarine variability* (pp. 341–353). Academic Press.

Pritchard, D. W. (1952). Salinity distribution and circulation in the Chesapeake Bay estuarine system. *Journal of Marine Research*, *11*(2), 106–123.

Ralston, D. K., Geyer, W. R., & Lerczak, J. A. (2008). Subtidal salinity and velocity in the hudson river Estuary: Observations and modeling. *Journal of Physical Oceanography*, *38*(4), 753–770. https://doi.org/10.1175/2007JPO3808.1

Rayson, M. D., Gross, E. S., Hetland, R. D., & Fringer, O. B. (2017). Using an isohaline flux analysis to predict the salt content in an unsteady Estuary. *Journal of Physical Oceanography*, *47*(11), 2811–2828. https://doi.org/10.1175/JPO-D-16-0134.1

Scully, M. E., Friedrichs, C., & Brubaker, J. (2005). Control of estuarine stratification and mixing by wind-induced straining of the estuarine density field. *Estuaries*, *28*(3), 321–326. https://doi.org/10.1007/BF02693915

Shchepetkin, A. F., & McWilliams, J. C. (2003). A method for computing horizontal pressure-gradient force in an Oceanic model with a nonaligned vertical coordinate. *Journal of Geophysical Research*, *108*(C3), 3090. https://doi.org/10.1029/2001JC001047

Shchepetkin, A. F., & McWilliams, J. C. (2009). Correction and commentary for "Ocean forecasting in terrain-following coordinates: Formulation and skill assessment of the regional ocean modeling system" by Haidvogel et al. *Journal of Computational Physics*, *227*, 3595–3624. https://doi.org/10.1016/j.jcp.2009.09.002

Stanley, D. W. (1992). Historical trends: Water quality and fisheries, Albemarle-Pamlico sounds, with emphasis on the pamlico river Estuary.

Stanley, D. W., & Nixon, S. W. (1992). Stratification and bottom-water hypoxia in the Pamlico River estuary. *Estuaries*, *15*(3), 270–281. https://doi.org/10.2307/1352775

Sutherland, D. A., MacCready, P., Banas, N. S., & Smedstad, L. F. (2011). A model study of the Salish Sea estuarine circulation. *Journal of Physical Oceanography*, *41*(6), 1125–1143. https://doi.org/10.1175/2011JPO4540.1

Sutton, J. N., Johannessen, S. C., & Macdonald, R. W. (2013). A nitrogen budget for the strait of Georgia, British Columbia, with emphasis on particulate nitrogen and dissolved inorganic nitrogen. *Biogeosciences*, *10*(11), 7179–7194. https://doi.org/10.5194/bg-10-7179-2013

Sylaios, G. K., Tsihrintzis, V. A., Akratos, C., & Haralambidou, K. (2006). Quantification of water, salt and nutrient exchange processes at the mouth of a mediterranean coastal lagoon. *Environmental Monitoring and Assessment*, *119*(1–3), 275–301. https://doi.org/10.1007/s10661-005-9026-3

Tully, K., Gedan, K., Epanchin-Niell, R., Strong, A., Bernhardt, E. S., BenDor, T., et al. (2019). The invisible flood: The chemistry, ecology, and social implications of coastal saltwater intrusion. *BioScience*, *69*(5), 368–378. https://doi.org/10.1093/biosci/biz027

Umlauf, L., & Burchard, H. (2003). A generic length-scale equation for geophysical turbulence models. *Journal of Marine Research*, *61*(2), 235–265. https://doi.org/10.1357/002224003322005087

Valle-Levinson, A., Delgado, J. A., & Atkinson, L. P. (2001). Reversing water exchange patterns at the entrance to a semiarid coastal lagoon. *Estuarine, Coastal and Shelf Science*, *53*(6), 825–838. https://doi.org/10.1006/ecss.2000.0813

Wang, D. P. (1979). Wind-driven circulation in the Chesapeake Bay, winter, 1975. *Journal of Physical Oceanography*, *9*(3), 564–572. https://doi.org/10.1175/1520-0485(1979)009<0564:wdcitc>2.0.co;2

Wang, T., Geyer, W. R., & MacCready, P. (2017). Total exchange flow, entrainment, and diffusive salt flux in estuaries. *Journal of Physical Oceanography*, *47*(5), 1205–1220. https://doi.org/10.1175/jpo-d-16-0258.1

Warner, J. C., Armstrong, B., He, R., & Zambon, J. B. (2010). Development of a coupled ocean–atmosphere–wave–sediment transport (COAWST) modeling system. *Ocean Modelling*, *35*(3), 230–244. https://doi.org/10.1016/j.ocemod.2010.07.010

Warner, J. C., Geyer, W. R., & Lerczak, J. A. (2005). Numerical modeling of an estuary: A comprehensive skill assessment. *Journal of Geophysical Research*, *110*(C5). https://doi.org/10.1029/2004JC002691

Warner, J. C., & Kalra, T. S. (2022). Collection of COAWST model forecast for the US east Coast and Gulf of Mexico. *U.S. Geological Survey data release*. https://doi.org/10.5066/P903KPBJ

Warner, J. C., Sherwood, C. R., Signell, R. P., Harris, C. K., & Arango, H. G. (2008). Development of a three-dimensional, regional, coupled wave, current, and sediment-transport model. *Computers and Geosciences*, *34*(10), 1284–1306. https://doi.org/10.1016/j.cageo.2008.02.012

Wells, J. T., & Kim, S. Y. (1989). Sedimentation in the albemarle-pamlico lagoonal system: Synthesis and hypotheses. *Marine Geology*, *88*(3–4), 263–284. https://doi.org/10.1016/0025-3227(89)90101-1

Woods, W. J. (1967). Hydrographic studies in Pamlico Sound. In *Proceedings of symposium on hydrology of the coastal waters of North Carolina* (pp. 105–114). Water Resources Research Institute, University of North Carolina.

Wu, H., & Zhu, J. (2010). Advection scheme with 3rd high-order spatial interpolation at the middle temporal level and its application to saltwater intrusion in the Changjiang Estuary. *Ocean Modelling*, *33*(1–2), 33–51. https://doi.org/10.1016/j.ocemod.2009.12.001

Xie, L., & Eggleston, D. B. (1999). Computer simulations of wind-induced estuarine circulation patterns and estuary-shelf exchange processes: The potential role of wind forcing on larval transport. *Estuarine, Coastal and Shelf Science*, *49*(2), 221–234. https://doi.org/10.1006/ecss.1999.0498

Xie, L., & Pietrafesa, L. J. (1999). Systemwide modeling of wind and density driven circulation in croatan-albemarle-pamlico Estuary system part I: Model configuration and testing. *Journal of Coastal Research*, 1163–1177.

Xie, X., & Li, M. (2018). Effects of wind straining on estuarine stratification: A combined observational and modeling study. *Journal of Geophysical Research: Oceans*, *123*(4), 2363–2380. https://doi.org/10.1002/2017JC013470

Xiong, J., MacCready, P., & Leeson, A. (2024). Impact of estuarine exchange flow on multi-tracer budgets in the Salish Sea. *Authorea Preprints*.

Xiong, J., Shen, J., Qin, Q., & Du, J. (2021). Water exchange and its relationships with external forcings and residence time in Chesapeake Bay. *Journal of Marine Systems*, *215*, 103497. https://doi.org/10.1016/j.jmarsys.2020.103497

Xu, H., Lin, J., & Wang, D. (2008). Numerical study on salinity stratification in the pamlico river Estuary. *Estuarine, Coastal and Shelf Science*, *80*(1), 74–84. https://doi.org/10.1016/j.ecss.2008.07.014

Yin, D., Harris, C. K., & Warner, J. C. (2025). A model archive for estuarine exchange flow in the albemarle-pamlico estuarine system [Dataset]. *William & Mary Scholar Works*. https://doi.org/10.25773/h1q6-pr14